

Final Scientific/Technical Report DOE Award No. DE-SC0018614, SBIR Phase I

Project Title: Field Compensation in Electron-Ion Collider Magnets With Passive Superconducting Shield

Report Date: 01/22/2019

Report Number: DOE-PBL-20190122

Company Name: Particle Beam Lasers, Inc.

Principal Investigator: Shailendra Chouhan

Purpose of Research, Research Carried Out, and Research Findings:

The Nuclear Science Advisory Committee (NSAC) constituted by the Department of Energy (DOE) Office of Nuclear Physics (NP) recommended that the proposed Electron Ion Collider (EIC) be the highest priority for new construction in the 2015 Long Range Plan (LRP) for Nuclear Science. The EIC requires development of several key technologies. To achieve high luminosity, Interaction Region (IR) designs need a high field quadrupole for the heavier proton beams and an almost field free path (desired magnetic field within a few mT) for the electron beams. The electron beam must travel very close to the quadrupole and dipole of the proton beams in the EIC but must be magnetically shielded from the external fields of those magnets.

The present EIC design is based on active shielding with additional superconducting coils opposing the field of the main magnets to obtain a field free region for passage of the electron beam. Our Phase I proposal was based on an alternate technique where a field free region for the electron beam is created by passive superconducting shielding which naturally creates a field free region and provides a cheaper and more efficient solution.

Significant progress has been made by the PBL and BNL team, including key demonstrations, some beyond the original scope of Phase I. In addition to analyzing the computer models of specific magnets, we also summarized the extensive experimental test results of several options for the superconducting shielding. These include 77 K tests of (a) two configurations of High Temperature Superconducting (HTS) ReBCO tape and (b) two orientations of tube made with HTS bulk material (Bi2223). Existing HTS coils were used in making a C-shaped dipole magnet to perform some of these tests. A practical advantage of HTS is that the basic shielding configuration can be tested at 77 K within the limited budget of Phase I.

In addition to 77 K tests with HTS, we were also able to perform rudimentary ~4 K tests with an HTS tube and with an LTS tube, which was beyond the tasks listed in the Phase I proposal. This was possible thanks to a synergy with another ongoing magnet test at BNL which could accommodate such shielding tests. These limited ~4 K tests are valuable and more realistic since the EIC magnets themselves will operate at ~4 K.

Potential Applications of the Research:

The primary application of the research is to enable studies of fundamental physics in an electron-ion collider (EIC). Effective shielding of the electron beam path from the high field magnets of the proton or ion beam is critical to the success of the EIC. The technology developed in Phase II will also be valuable in the development of superconducting magnets for other research and commercial applications.

Final Scientific/Technical Report DOE Award No. DE-SC0018614, SBIR Phase I

Recipient: Particle Beam Lasers, Inc.
18925 Dearborn Street
Northridge, CA 91324-2807

Sponsoring Program Office: Office of Science
U.S. Department of Energy

Project Title: Field Compensation in Electron-Ion Collider Magnets
With Passive Superconducting Shield

Principal Investigator: Shailendra Chouhan, PBL

Team Members: Ramesh Gupta, BNL
Shresht Joshi, BNL
Paul Kovach, BNL
William Sampson, BNL
Stephen Kahn, PBL
James Kolonko, PBL
Delbert Larson, PBL
Ronald M. Scanlan, PBL
Robert Weggel, PBL
Erich Willen, PBL

SBIR/STTR Rights Notice (JAN 2015)

These SBIR/STTR data are furnished with SBIR/STTR rights under Award No. DE-SC0018614. Unless the Government obtains permission from the Recipient otherwise, the Government will protect SBIR/STTR data from non-governmental use and from disclosure outside the Government, except for purposes of review, for a period starting at the receipt of the SBIR/STTR data and ending after 4 years, unless extended in accordance with 48 CFR 27.409(h), from the delivery of the last technical deliverable under this award. In order for SBIR/STTR data to be extended by an SBIR/STTR Phase III award, the Recipient must properly notify DOE's Office of Scientific and Technical Information (OSTI) before the end of the previous protection period. After the protection period, the Government has a paid-up license to use, and to authorize others to use on its behalf, these data for Government purposes, but is relieved of all disclosure prohibitions and assumes no liability for unauthorized use of these data by third parties. This notice shall be affixed to any reproductions of these data, in whole or in part.

(End of notice)

Acknowledgment: This material is based upon work supported by the U.S. Department of Energy, Office of Science under Award Number DE- SC0018614.

Disclaimer: This report was prepared as an account of work sponsored by an agency of the United States Government. Neither the United States Government nor any agency thereof, nor any of their employees, makes any warranty, express or implied, or assumes any legal liability or responsibility for the accuracy, completeness, or usefulness of any information, apparatus, product, or process disclosed, or represents that its use would not infringe privately owned rights. Reference herein to any specific commercial product, process, or service by trade name, trademark, manufacturer, or otherwise does not necessarily constitute or imply its endorsement, recommendation, or favoring by the United States Government or any agency thereof. The views and opinions of authors expressed herein do not necessarily state or reflect those of the United States Government or any agency thereof.

Table of Contents

Final Scientific/Technical Report DOE Award No. DE-SC0018614, SBIR Phase I	1
Table of Contents	4
1.0 Introduction.....	5
2.0 Current Technical Approach.....	5
3.0 Magnet Design Analysis	5
3.1 Section A: Cosine Two Theta Q1PF Magnet 2D and 3D Design.....	8
3.2 Section B: Cosine Two Theta QFFUS_1 Magnet 2D and 3D Design	16
4.0 Superconducting Shielding Options	20
5.0 Superconducting Shielding Tests.....	21
5.1 Shielding Tests with Spirally Wound HTS Tape at 77 K	23
5.2 Shielding Tests with Axially Wrapped HTS Tape at 77 K	25
5.3 Shielding Tests with HTS Tube at 77 K	26
5.4 Shielding Tests with HTS and LTS Tubes at 4 K.....	29
6.0 Prospects of Shielding in Various EIC Magnets.....	31
7.0 Planning of the Shielding Tests in Phase II	33
8.0 Summary	35
9.0 References.....	36

1.0 Introduction

This report summarizes findings of design work performed under the Small Business Innovation Research (SBIR) Phase I grant (DE-SC0018614) to Particle Beam Lasers, Inc. (PBL) and Brookhaven National Laboratory (BNL) to develop passive superconducting shielding as an alternative to the present design of an active shield with superconducting coils. This passive shielding will provide a nearly field-free region for the electron beam near the high-gradient quadrupole for the proton beam in the Interaction Region (IR) of the proposed Electron Ion Collider (EIC) [1-6]. Several materials are being examined for this shielding: tubes of low- or high-temperature superconductors (LTS or HTS), and HTS tapes. In addition, to enhance the magnetic shielding, we propose employing an iron tube between the superconducting shield and beam tube to counter any decay in shielding currents of the superconducting shield. If successfully developed, demonstrated and shown to be compatible with the magnet designs of all the IR magnets, this technique will provide an economical and technically excellent solution that reduces the operating current needed by the IR magnets. The report summarizes the latest design studies and test results both at 77 K for the shielding by the HTS (tube and tapes) and at 4 K for the shielding by tubes of HTS or LTS.

2.0 Current Technical Approach

In the current approach, the BNL interaction region quadrupole (Q1PF) design is based on a conventional Cosine Two Theta design [7]. To shield the nearby electron beam from the fringe field of the magnet, the Cosine Two Theta design is shielded actively [7]. Nb_3Sn conductor is needed for the main coils, to provide the required field gradient; NbTi suffices for the field-cancelling coils that achieve the field-free region for the electron beam. The cross-section of the actively shielded BNL Q1PF is shown in Fig. 1.

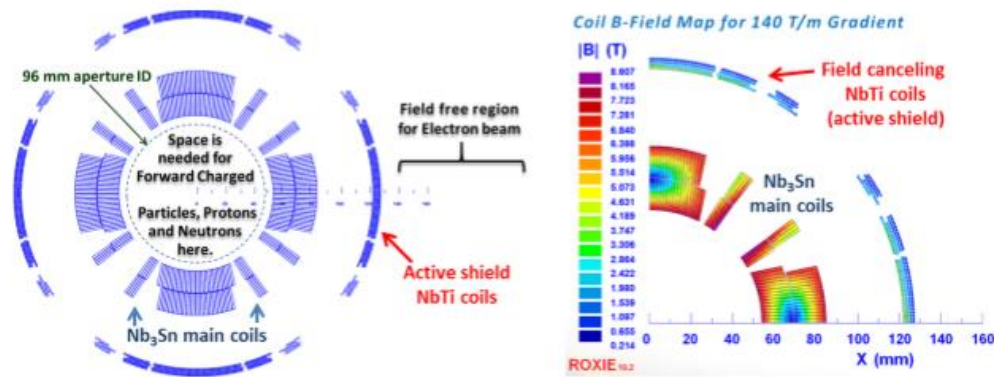


Fig. 1: The existing design of Q1PF quadrupole [7] for the BNL design of the EIC (eRHIC), showing the main Nb_3Sn coils and the field-cancelling NbTi coils: full cross-section on the left; a quadrant with field contour on the surface of main and shielding coils on the right.

3.0 Magnet Design Analysis

Magnetic shielding is needed in the EIC IR magnets of both the BNL and the JLAB proposal. For the BNL-proposed EIC Interaction Region (IR), the electron beam requires magnetic shielding from the fringe field of the large-aperture ion-beam-focusing quadrupole (example Q1PF) [7]. We performed magnetic design calculations for the BNL_Q1PF quadrupole, which requires a high field

gradient, a low field region and a compact design, due to the nearby electron beam line. The design parameters of the magnets at various stages of BNL and JLAB program are shown in Tables I to III [6, 8]. The design optimization has been carried out for the Q1PF quadrupole with the return yoke of Table I. The object of this yoke optimization is to ensure that along with the field gradient there is a nearly-field-free region for the passage of the electron beam in the interaction region [IR] of the EIC with the inclusion of passive shielding such as *LTS/HTS material and low carbon ferromagnetic material*. Various suitable materials for this application will be discussed in later sections of the report. The purpose to add a thin tube of *ferromagnetic material* of low retentivity between the superconducting shielding tube and the electron-beam tube is to maintain the effectiveness of the passive shielding despite decay currents or transient effects of the superconductor.

For the JLAB EIC Interaction Region [8], the section enclosed by the blue dashed line is an area of interest in which magnetic shielding via passive superconducting material could be assumed, as shown in Fig. 2. In this section, shielding is required to isolate the ion beam from the stray field of the electron beam line quadrupole. The most critical quadrupole that needs shielding is the closest to the interaction point for focusing the electron beam at the front end. The quadrupole QFFUS_1 is the closest electron beam line quadrupole and only few meters away from the central detector solenoid. The magnetic design study has been performed for the QFFUS1 and discussed in detail in later sections of the report. In the section of the Interaction Region (IR) enclosed by the red rectangle the proposed scheme of using a superconducting passive shield over the electron beam tube for the field free region is not an option. As per current lattice designs, electron-beam focusing magnets are needed in those locations [6-8]. The details of the interaction region layout are shown in the Fig.2. In the section of the IR region enclosed by the red rectangle, large-aperture, high-field-gradient (120-150 T/m) focusing quadrupoles are needed for the ion beam, along with the regular focusing quadrupole (45 T/m) for the electron beam. The design parameters of the JLEIC Interaction Region (IR) quadrupole magnets for the electron beam line are shown in Table III; requirements of the QFFUS_1 quadrupole are highlighted.

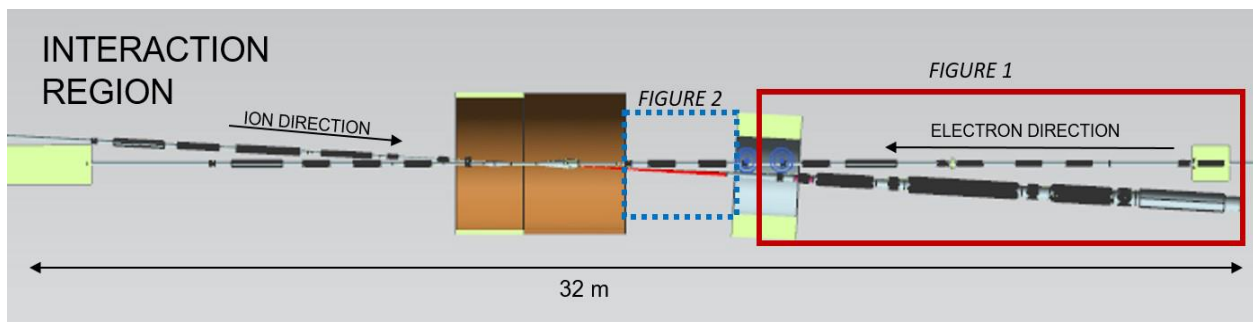


Fig.2. JLab's EIC Interaction Region layout (courtesy: Dr. Renuka Rajput) [8].

Irrespective of the beam type (ion or electron) that needs shielding from the stray field of the nearby magnets, the shielding will benefit magnet designs in the EIC IR magnets of both the BNL and the JLAB proposals. We performed magnetic design studies for the BNL ion beam quadrupole Q1PF and JLAB's electron beam transport line quadrupole QFFUS_1.

Table I: Design Parameters of BNL EIC Interaction Region Magnets (October 2017)

Hadron Forward Side							
Name	Beam	Position entrance[m]	Length [m]	Strength	Full Aperture entrance [mm]	Full Aperture exit [mm]	Coil Type
B0PF	hadrons	5.	1.2	1.3 T	500× 240	500×240	s.c.NbTi
Q1EF	electrons	5.0	1.2	14.6 T/m	22	22	s.c. NbTi
Q1PF	hadron	6.8	1.5	131 T/m	84	84	s.c. Nb ₃ Sn
Q1PF Shield	electrons	6.8	1.5	N/A	N/A	N/A	s.c. NbTi
Q2EF	electrons	8.74	1.72	6.0 T/m	48.5	48.5	s.c. NbTi
Q2PF	hadrons	11.1	2.4	45 T/m	210	210	s.c. NbTi
B1PF	hadrons	13.9	3.0	4.47 T	204	244	s.c. NbTi
Hadron Rear Side							
Name	Beam	Position [m]	Length [m]	Strength	Full Aperture entrance [mm]	Full Aperture exit [mm]	Coil Type
Q1ER	electrons	5.5	3.42	5.1 T/m	135	186	s.c. NbTi
Q1PR	hadrons	5.5	3.42	82.9 T/m	42	68	s.c.NbTi
Q2ER	electrons	11.67	2.57	4.23 T/m	228	266	s.c.NbTi
Q2PR	hadrons	11.67	2.57	54.86 T/m	90	110	s.c.NbTi
B2ER	electrons	19.2	4.0	0.09 T	281	338	s.c.NbTi

Table II: Current Design Parameters of BNL EIC Interaction Region Magnets (October 2018)

Hadron Forward Side							
Name	Beam	Position entrance [m]	Length [m]	Strength	Full Aperture entrance [mm]	Full Aperture exit [mm]	Coil Type
B0PF	hadrons	5.30	1.20	1.3 T	500 x 240 (HxV)	500 x 240 (HxV)	s.c. NbTi
Q0EF	electrons	5.30	1.20	-13 T/m	26.0	26.0	s.c. NbTi
Q1APF	hadrons	7.00	1.46	-78 T/m	45.0	45.0	s.c. NbTi
Q1BPF	hadrons	8.76	1.61	-63 T/m	65.0	65.0	s.c. NbTi
Q1EF	electrons	8.76	1.61	1.7 T/m	46.4	58.0	s.c. NbTi
Q2PF	hadrons	11.27	3.60	40 T/m	108.0	108.0	s.c. NbTi
Q2EF	electrons	11.27	2.00	3.8 T/m	63.5	63.5	s.c. NbTi
B1PF	hadrons	15.37	3.00	4.57 T	125.0	125.0	s.c. NbTi
Hadron Rear Side							
Name	Beam	Position entrance [m]	Length [m]	Strength	Full Aperture entrance [mm]	Full Aperture exit [mm]	Coil Type
Q1APR	hadrons	5.30	1.80	-79 T/m	20.1	27.7	s.c. NbTi
Q1ER	electrons	5.30	1.80	-13 T/m	66.0	79.5	s.c. NbTi
Q1BPR	hadrons	7.60	1.40	-79 T/m	30.0	30.0	s.c. NbTi
Q2ER	electrons	7.60	1.40	13 T/m	83.2	93.8	s.c. NbTi
B2ER	electrons	9.50	5.50	0.18 T	97.5	138.8	s.c. NbTi
Q2PR	hadrons	11.00	2.00	74 T/m	50.0	50.0	s.c. NbTi

Table III: Design Parameters of JLAB EIC Interaction Region Magnets

Magnet Location	Magnet Type	JLAB Requirements						Angle between ion & electron beam line (mrad)
		Magnet Strength	Magnetic length	Distance from the	Good field	New Inner Radius	Outer radius (cm)	
Interaction Region Ion (IR)	Quadrupole QFFB3_US	-116	1	-7.70	3 cm	4	12	50
	Quadrupole QFFB2_US	149	1.5	-6.00	3 cm	4	12	50
	Quadrupole QFFB1_US	-141	1.2	-4.20	2 cm	3	10	50
	Quadrupole QFFB1	-88	1.2	7.60	4 cm	8.5	17.1	50
	Quadrupole QFFB2	51	2.4	10.40	4 cm	12.6	24.7	50
	Quadrupole QFFB3	-35	1.2	13.20	4 cm	14.8	26.7	50
Interaction Region Electron (IR)	Common Quad design based on new requirement January 2018, combined with Skew Quads	Quad 45 (varies from 13.63 to 44.78)	0.6	-4.9 -3.7 -2.5 3.26 4.46 6.91	3.2	4.5	8	50

3.1 Section A: Cosine Two Theta Q1PF Magnet 2D and 3D Design

The Q1PF is the most critical quadrupole and is the closest to the interaction point for focusing the proton (ion) beam at the front end. The nearby electron beam needs shielding from the stray field of the Q1PF quadrupole. The OPERA simulation software from Dassault Systèmes [9] has been used for most electromagnetic 2D and 3D simulations supplemented by the ROXIE from CERN [10]. The parametric finite element model began as 2D, to minimize time-intensive 3D calculations. The mass of the yoke was optimized within the physical constraints; the cross-section of the superconducting coil is identical to the cosine two theta design. Optimized was the return yoke with a cutout to minimize the fringe field magnitude while preserving field quality over the operating range. Fig. 3 shows the optimized cross-section of the BNL design Q1PF, with 96-mm-aperture Nb₃Sn superconducting coils providing a field gradient of 168 T/m (140 T/m + 20% margin), and a cutout in the iron yoke providing passage for the electron beam. The electron beam is at a small angle from the proton (ion) beam.

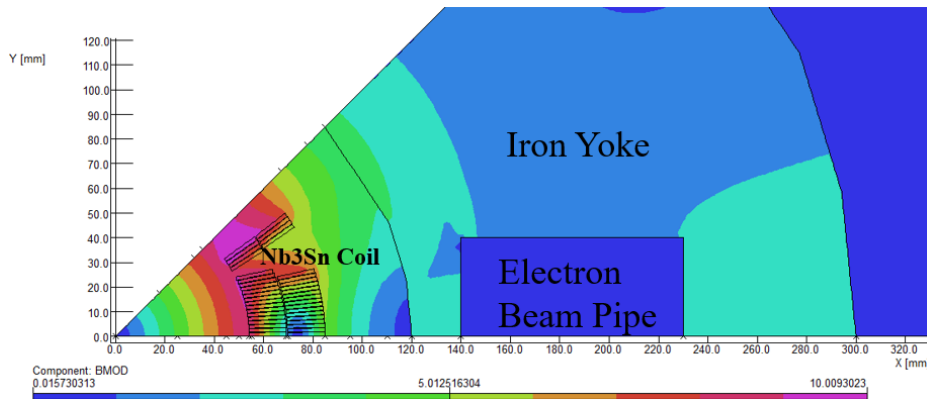


Fig.3. OPERA2d model of Q1PF quadrupole design with Nb₃Sn superconducting coils and the optimized return yoke with rectangular cutout for the electron beam pipe.

The peak field magnitude in the coil is around 10 teslas; that in the iron is around 5.01 teslas. It also shows a reduced-field region in the cutout section of the return yoke for the electron beam. The yoke cross-section is optimized to minimize the field magnitude in the electron beam region; the calculated field in the beam region is 0.2 to 0.3 T. The maximum field in the corners of the slot

is around 0.85 T. The calculated field magnitude at the pole ($r = 0.036$ m) is 6.05 T. The model also provides values for the Lorentz forces on the coil, the stored energy and the magnitude of higher harmonics in the center of the magnet. The quadrupole field component (B_{MOD}) profile along the radial axis is shown in Fig. 4a, with an enhanced scale in the region of interest in Fig. 4b. The linear field region (168 T/m) in the center of the magnet provides the required focusing for the proton/ion beam.

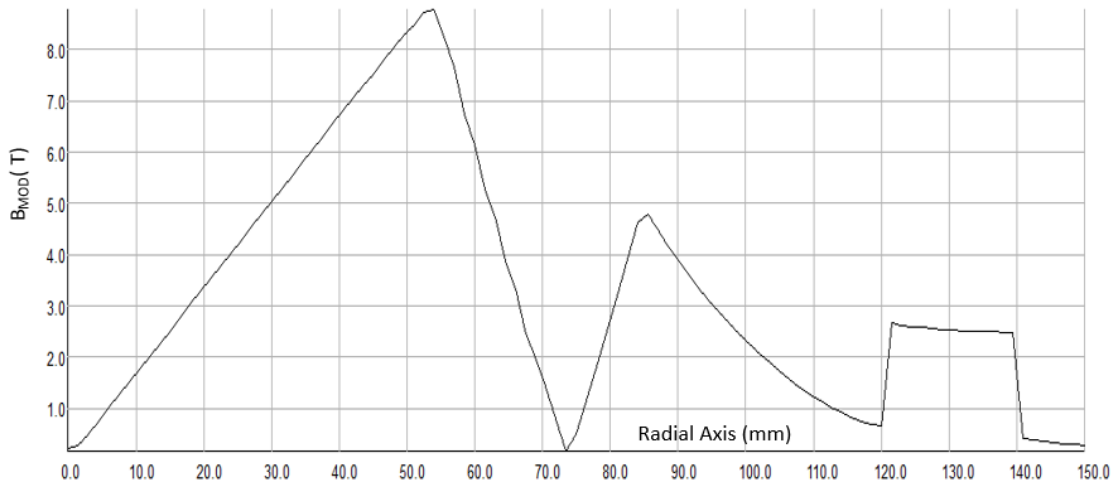


Fig.4a. Profile of the calculated field component (B_{MOD}) along the radial axis. The magnitude of the field at a radius of 0.036 m is 6.05 teslas.

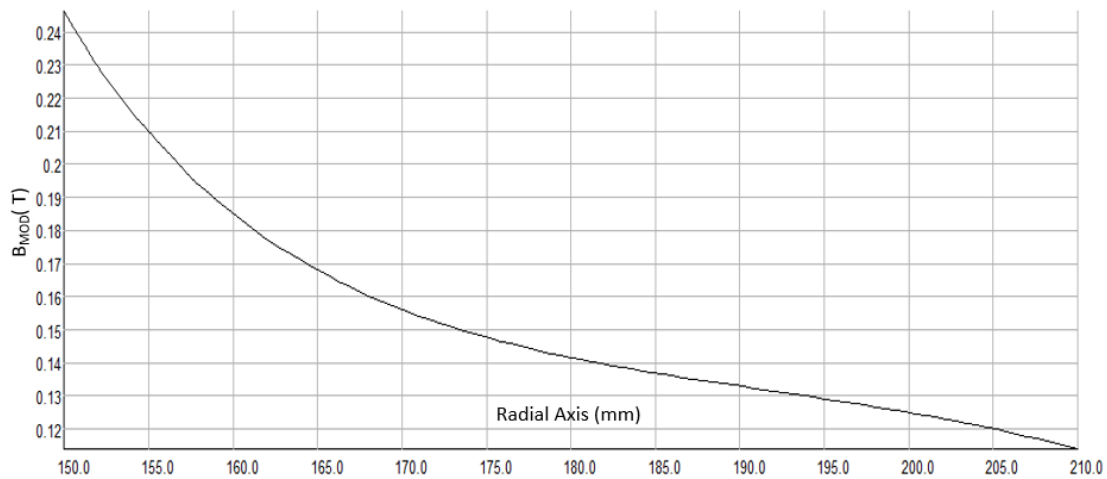


Fig.4b. Profile of the calculated field components (B_{MOD}) at mid-plane along the radial axis in the region of the electron beam axis (150 mm to 210 mm).

The exploded view of the cutout with field distribution is shown in Fig. 5. The field magnitude ranges from 0.2 T to 0.3 T within the electron beam region. The maximum field, in the corner of the cutout, is 0.85 T. The advantage of the return yoke is that it reduces, by 10% and 30% respectively, the operating current requirement and the fringe field along the beam axis. A comparison field plot in the region of electron beam for two cases, with and without return yoke, is shown in Fig. 6.

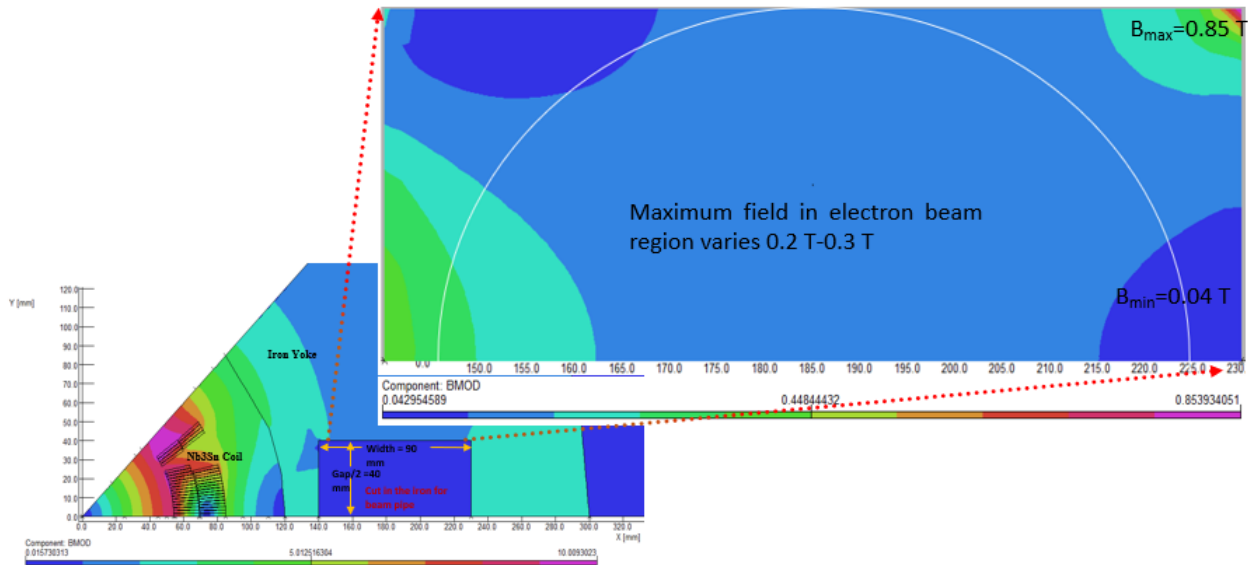


Fig.5. Exploded view of the cutout region. Peak field in the corners of the slot and magnitude is around 0.85 T. The maximum field in the electron beam region varies from 0.2 T to 0.3 T.

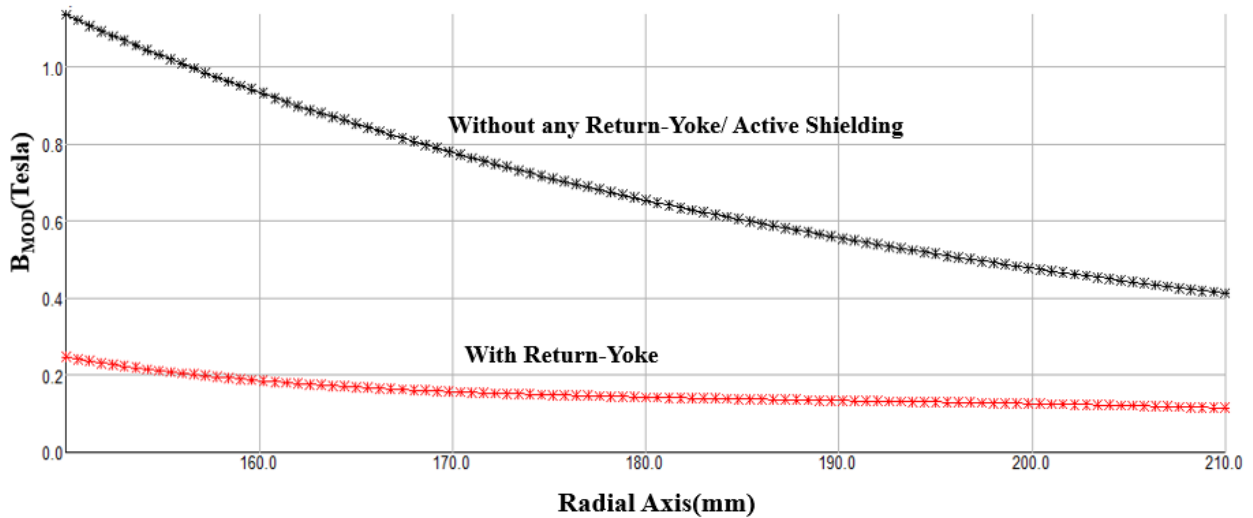


Fig.6. Exploded view of the cutout region. Peak field in the corners of the slot and magnitude is around 0.85 T. The maximum field in the electron beam region ranges from 0.2 T to 0.3 T.

A 3D model has been developed to analyze the impact of the return yoke on the field quality, *especially the stray field in and along the electron beam pipe*, the peak field in the coil area, the flux distribution along the beam axis, the integrated higher harmonic contents, and the forces on the coil. Fig. 7 shows the 1/16th 3D meshed model of the BNL_QIPF quadrupole with coils and the surrounding air region. Fig.8 shows a schematic layout for the quadrupole magnet, with coils and cutout in the return yoke (dimensions are in cm). Each quadrant of the magnet encompasses a set of four constant-end-parameter coil blocks angularly distributed with space for keys (G10 and high-strength material spacers) to contain the magnetic forces.

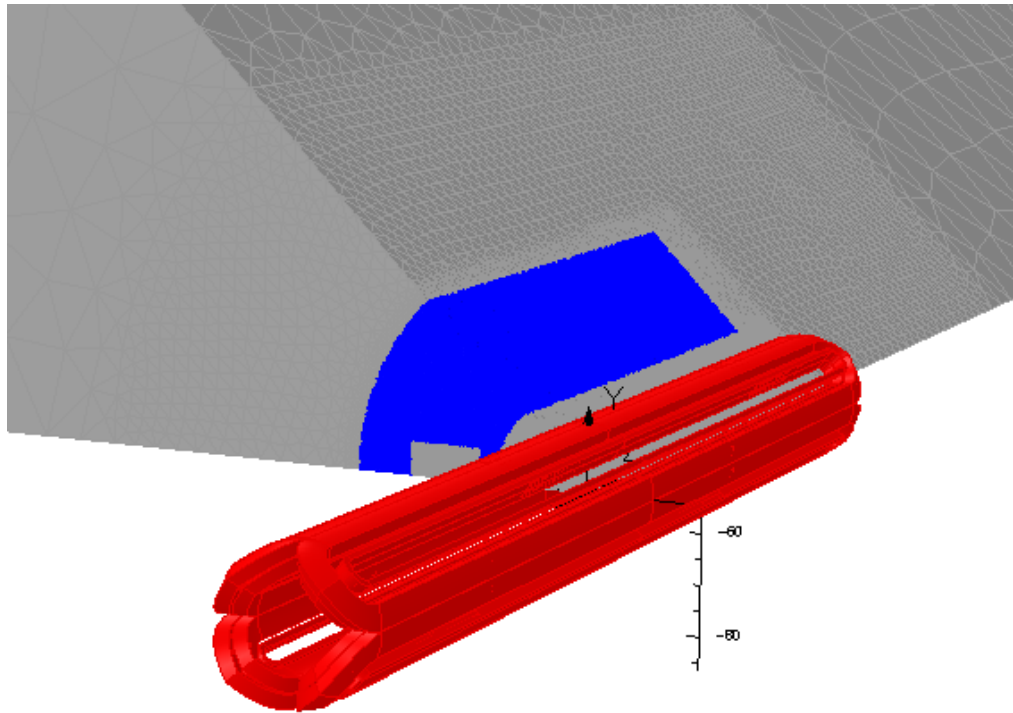


Fig.7. 3D meshed model for superconducting Q1PF quadrupole magnet with coils, return yoke and background air (dimensions are in cm).

Based on the 2D and 3D designs, detailed analyses have been performed and the important extracted results compared. Field contours on the surface of the Q1PF quadrupole conductor are shown in Fig.8. Both 2D and 3D results suggest a peak field magnitude of around 10.7 teslas on the conductor surface and 4.2 T in the return yoke. Field data (B_Y and B_{MOD}) along the radial axis of the 2D and 3D models are compared in Fig.9; results of the two models agree.

A full 3D model of the Q1PF, along with the electron beam pipe, is shown on the left side of Fig.10. In order to maintain symmetry, cutouts have been included in all four-quadrant. The electron beam pipe is at 180 mm from the center of the magnet. The field profile along the electron beam axis is shown on the right side of the Fig.10; the calculated field value is around 0.16 teslas. The field in the electron beam region is significantly higher and does not meet requirement.

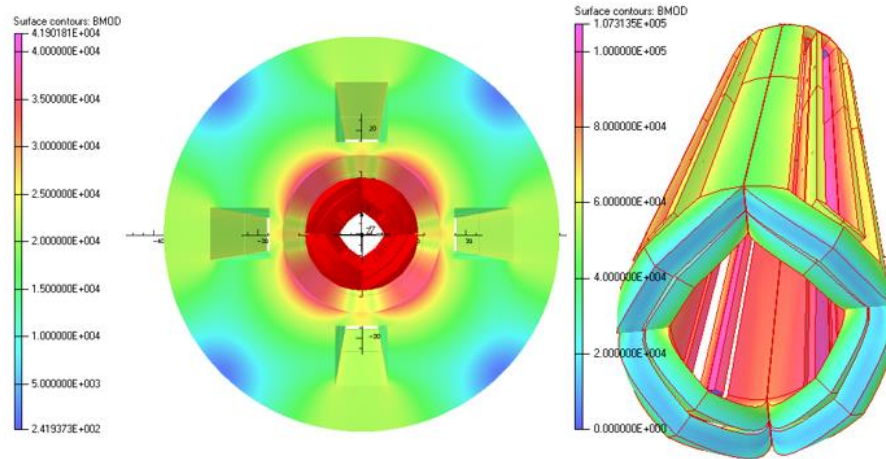


Fig.8. Schematic layout for superconducting Q1PF quadrupole magnet with full set of coils. The peak field magnitude in the iron is 4.2 T (left); the peak field on the superconductor is around 10.7 T.

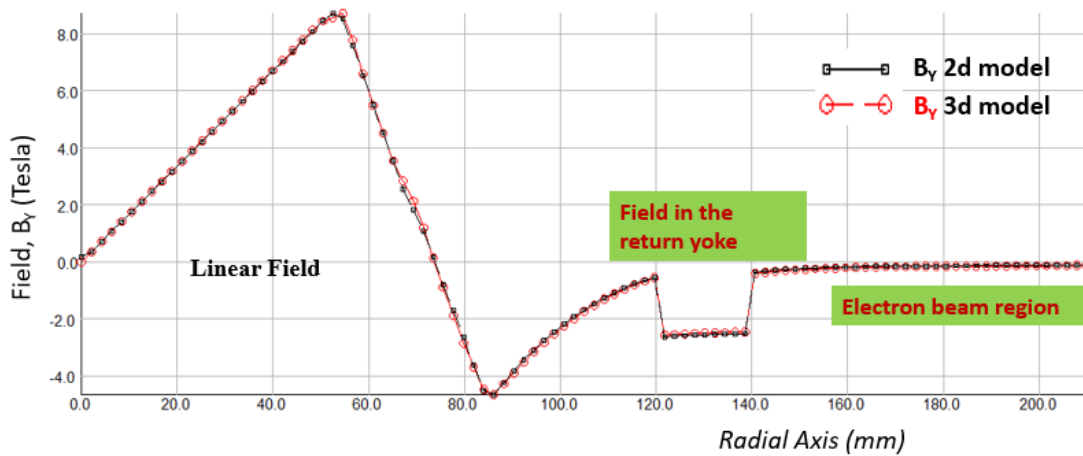


Fig.9a. Calculated field, B_y (T) results from 2D and 3D models compared along the radial axis. (Units are in millimeters and teslas).

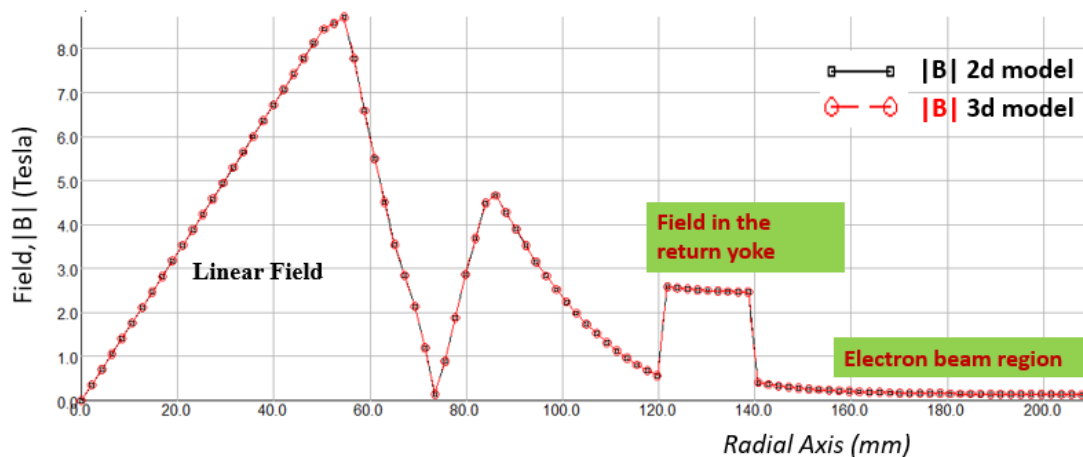


Fig.9b. Calculated field, B_{MOD} (T) results from 2d and 3d model compared along the radial axis. (Units are in millimeters and teslas).

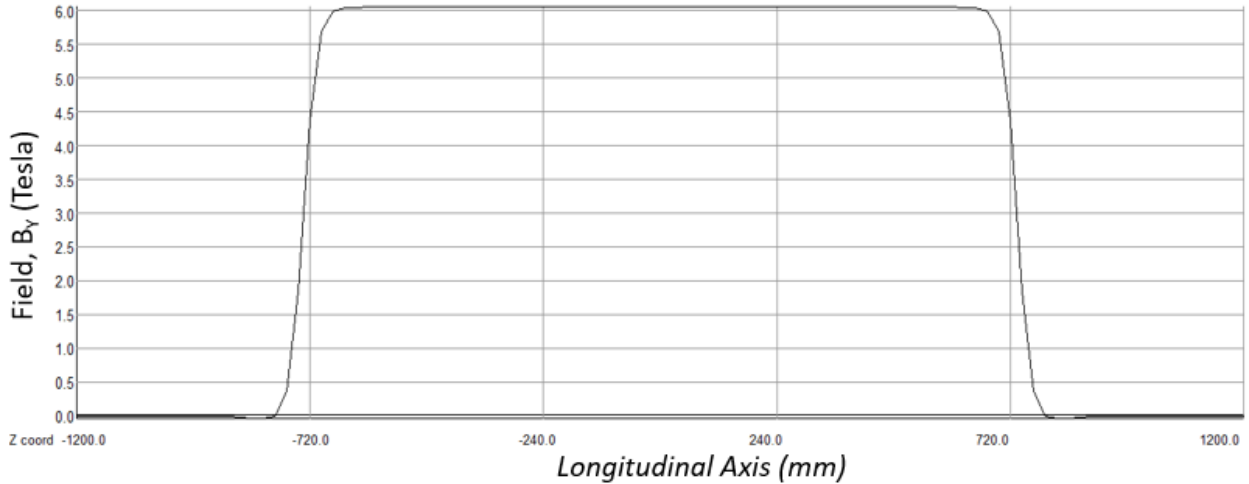


Fig.9c. Field (B_Y) plot along the longitudinal (ion beam) axis at a radius of 36 mm. Units are in millimeters and teslas.

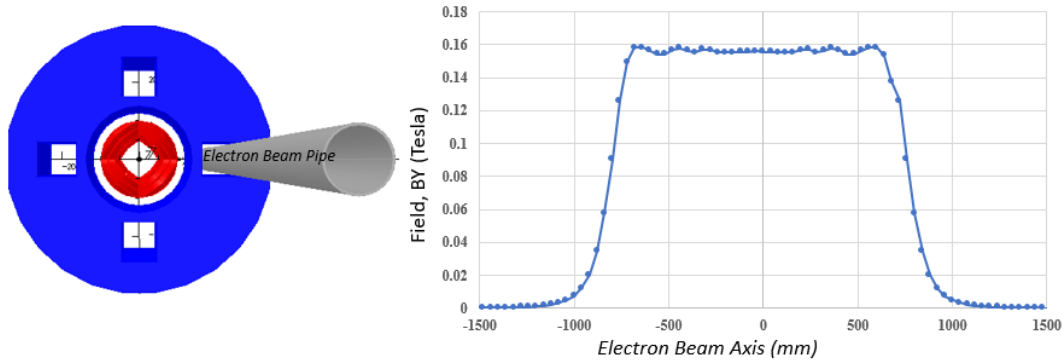


Fig.10. Full 3D model along with electron beam pipe at 180 mm from the magnetic center (on the left). Field plot along the electron beam axis (right). Units are in millimeters and teslas.

The above calculations and analysis reveal that although iron can help to contain the magnetic flux within the material and reduce the stray field magnitude significantly, as shown in Fig.6, it is not enough to create a region that is sufficiently free of field for the nearby electron beam. To achieve the desired result, a passive shield that combines a superconducting and high-permeability material (for example, μ -metal) is being considered. Compactness and being an integral part of the cold-mass (magnet) are added advantages of the cold shield. The similar concept of superconducting shielding has been applied in previous applications, such as the g-2 experiment [11] and a cloak experiment [12, 13]. The concept was also considered at DESY [14]. The proposed shielding option for a high-field septum magnet for the Future Hadron Collider is based on multi-layer (NbTi/Nb/Cu) superconducting material [15].

Superconducting shielding works because any change in ambient magnetic field induces currents in the shield, and these currents oppose the change of field inside the shield. In a simplified model to simulate the presence of the superconducting shield we have included a thin tube of very low permeability material ($\mu_0 \ll 1$). The program used (OPERA) has no way of setting the strength of

the field trapped inside the material as it cooled through its transition temperature. We assumed that shield is cooled to the superconducting state in zero external field; otherwise it would trap the initial field. A thin tube of high permeability material such as μ -metal (cryoperm) between the superconducting shield and beam tube preserves the effectiveness of the passive shielding despite decay currents or transient effects of the superconductor.

The computed maximum field in the upper-left corner is about 0.85 T; in the shielding region, it ranges from 0.2 to 0.3 T, as discussed previously (Figs. 4-6). This can be shielded by a superconducting shield made of either low temperature superconducting (LTS) or high temperature superconducting (HTS) material along with a ferromagnetic shield. Fig. 11 shows the field contour in the optimized BNL Q1PF model that includes the return yoke and passive shields (both superconducting and high-permeability material) in the cutout region. The bottom picture shows the field contour inside the cutout region (Fig. 12), with the passive superconducting and magnetic shield each 1 mm thick. The preliminary magnetic simulation results are encouraging. The model cross-section can be optimized later for updated magnet design parameters and based on the measurement results. The magnitude of field distributed inside the shielded region for the electron beam (as shown in Fig. 12) is essentially zero.

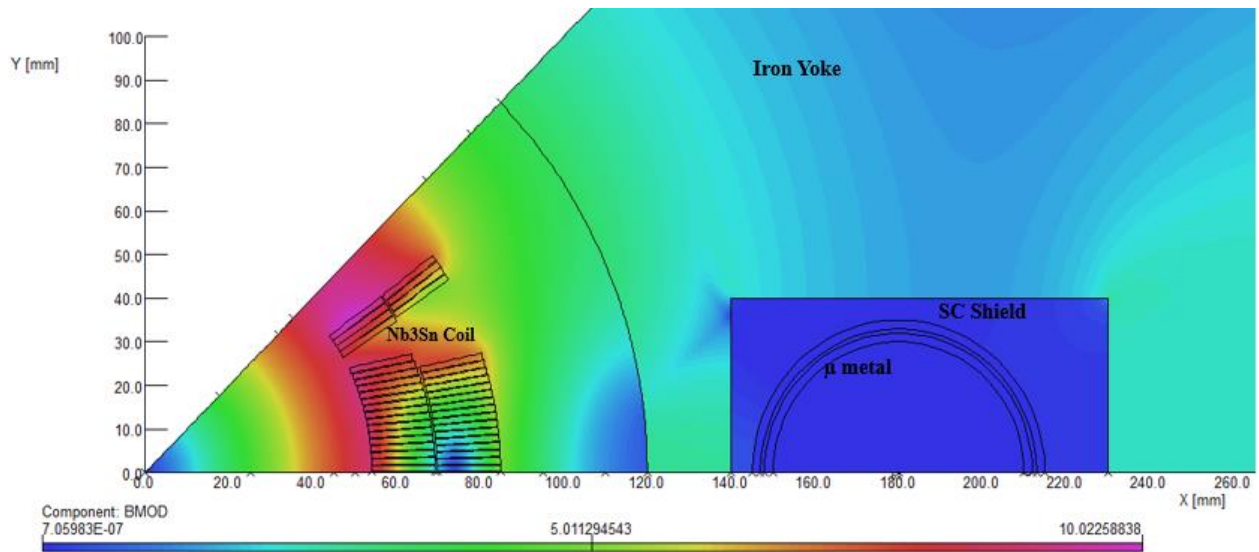


Fig.11. Field contour on the surface of QIPF OPERA2d model that includes passive shielding (both superconducting and magnetic) in the cutout region.

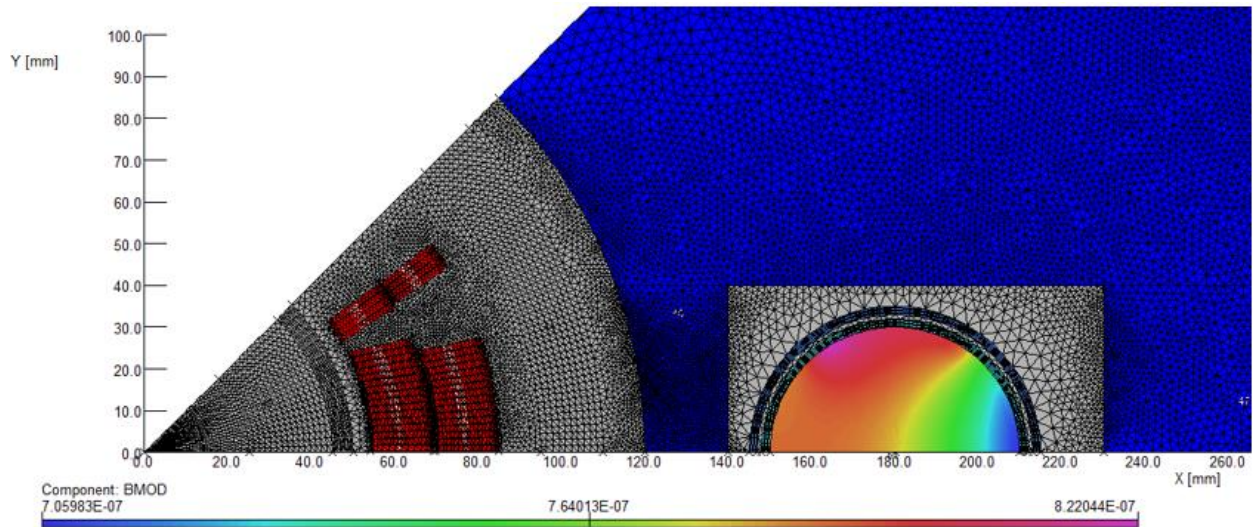


Fig.12. Field contour in the location of interest of Q1PF OPERA2d model that includes passive shielding (both superconducting and magnetic) in the cutout region. The field magnitude is nearly zero field in the region of electron beam.

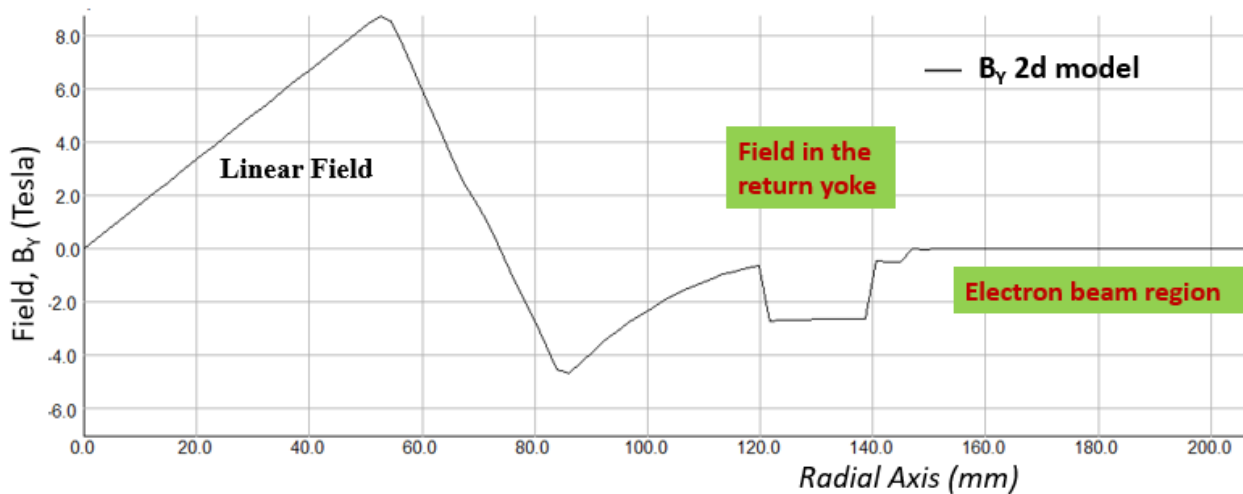


Fig.13. Profile of the calculated field components (B_Y) along the radial axis. The magnitude of the field at a radius of 0.036 m is 6.04, whereas magnitude of the field 180 mm is nearly zero.

In the coil configuration of the Q1PF design, the parameters of the proposed Nb_3Sn cable are identical to the cable previously used in the fabrication of a LARP quadrupole magnet [16]. The parameters of the Nb_3Sn cable are summarized in Table IV.

TABLE IV: Basic Conductor Parameters

Strand diameter (mm)	0.8
Cu to non-Cu ratio	1.17
Number of strands	35
Cable insulation (mm)	0.1
Cable width, bare (mm)	15.15
Mid-thickness (mm)	1.338
Keystone angle [degrees]	0.75
Cable width, insulated (mm)	15.35
Mid-thickness, insulated (mm)	1.637
Cable I_c (4.4 K, 13.54 T), A/mm ²	2087

3.2 Section B: Cosine Two Theta QFFUS_1 Magnet 2D and 3D Design

For the JLAB EIC Interaction region [8], the magnet QFFUS_1 for electron beam focusing is the closest magnet to the detector solenoid. The exploded view of the section enclosed by the blue dashed line is shown in Fig. 14; it is an area of interest for magnetic shielding via passive superconducting material. In this section, shielding is required for the ion beam from the stray field of the electron beam line quadrupole QFFUS_1. The quadrupole QFFUS_1 requires a peak gradient of 45 T/m; the distance of the center of the magnet from the central detector solenoid is 3.26 meter. Details of magnetic design parameters are listed in Table III; requirements of the electron beamline focusing quadrupole are highlighted. Fig. 14 portrays details of other large-aperture, high-gradient (120-150 T.m) quadrupole magnets for the ion beam focusing. The design parameters of all the JLEIC Interaction Region (IR) quadrupole magnets for the electron and ion beam line also are listed in Table III.

A 2D parametric finite element model for QFFUS_1 was created and an optimization performed to minimize the stray field in the ion beam region. The mass of the yoke and cross-section of the superconducting coil were optimized; the cross-sections of the JLAB QFFUS_1 is shown in Fig. 15. The coils are relatively compact and use NbTi-Cu matrix cable, with an engineering current density of about 280 A/mm². A constant perimeter end type coil configuration is used.

Fig. 16 shows an OPERA2d field contour plot for the QFFUS_1 quadrupole design. The design field gradient is 45 T/m; the coil aperture is 90 mm. The peak field magnitude in the coil is around 3.0 T, whereas the peak magnitude of the field in the iron is around (1.5 T). Fig. 16 also shows a reduced-field region in the cutout section of the return yoke for the ion beam. The ion beam pipe is conical flaring from 60 mm at its entrance (near the detector solenoid) to 90 mm and at its end. The rectangular cutout in the yoke accommodates the 2.865° angle between the two beam lines. The half-height of the rectangular cutout is 50 mm; the width is 96 mm. The yoke cross-section is optimized to minimize the field saturation in the iron and consequently minimizes the stray field in the ion beam region. The QFFUS_1 quadrupole model provides a field gradient of 49 T/m and a peak field at the pole ($r = 0.032$ m) of 1.57 T. The model also provides values for the Lorentz forces on the coil, the stored energy and the magnitude of higher harmonics in the center of the magnet.

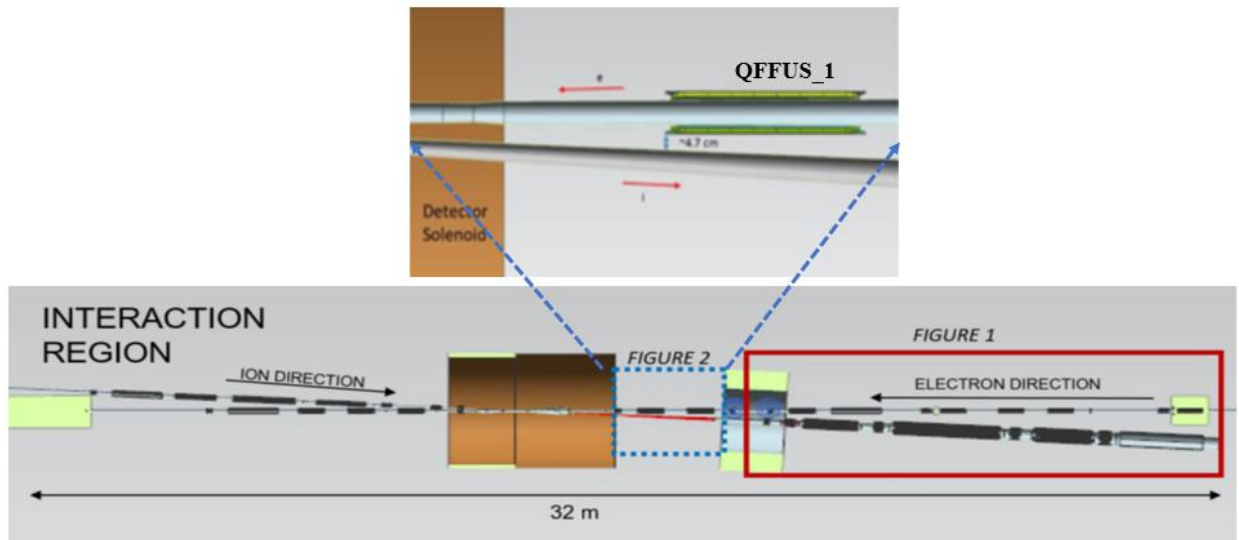


Fig.14. Jefferson National Lab's EIC Interaction Region layout. Electron beam line magnets in the exploded view of the section enclosed by the blue dashed line are close to the detector solenoid (courtesy: Dr. Renuka Rajput) [8].

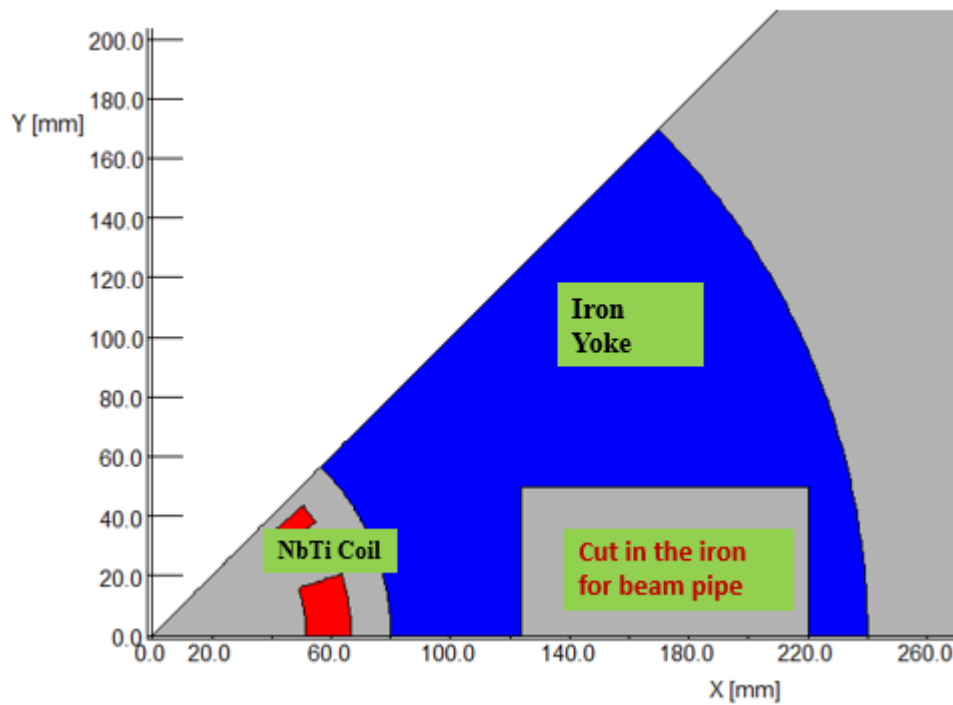


Fig.15. OPERA2d model of JLAB QFFUS_1 quadrupole design with optimized NbTi coils and rectangular cutout in the return yoke for the ion beam pipe.

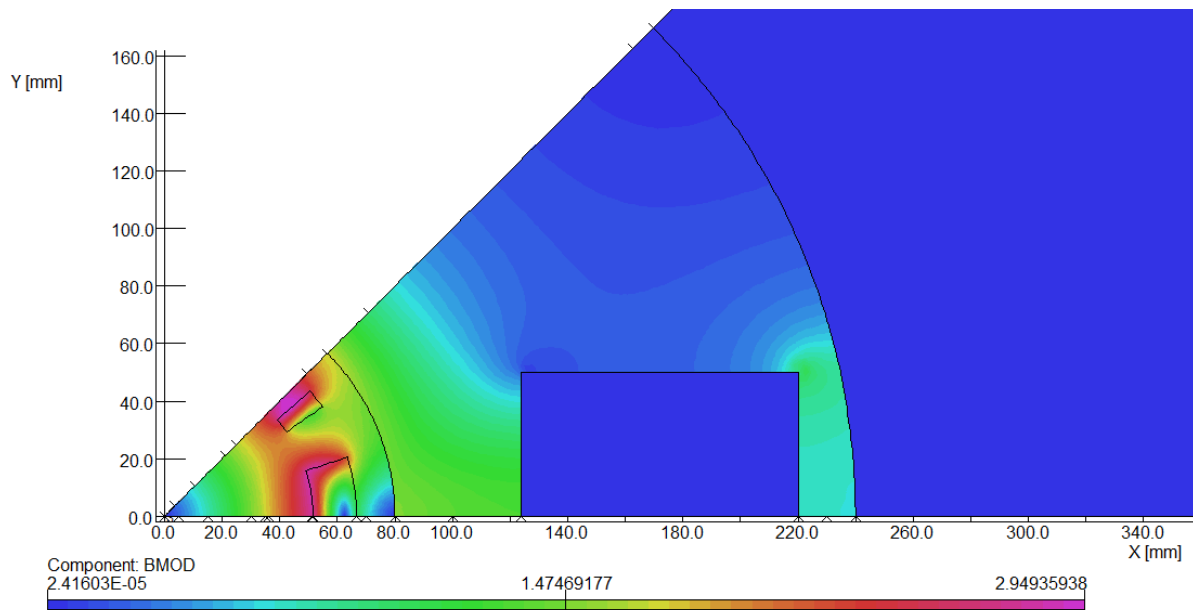


Fig.16. OPERA2d model of QFFUS_1 quadrupole design with NbTi superconducting coils and the optimized return yoke with rectangle cutout for the ion beam pipe.

The bottom picture shows the field contour inside the cutout region (Fig. 17), based on the preliminary calculation. The magnitude of field distributed inside the cutout region for the ion beam is in the range of 10^{-4} T. The result suggests it meets the requirements [8], has ample possibilities for further optimization, and even can be reduced to nearly zero field by adding a passive superconducting shield if needed. The quadrupole field components (BY and BMOD) profile along the radial axis are shown in Fig. 18. The linear field region in the center of the magnet provides the required field gradient (49 T/m) for the electron beam. Calculated field magnitude at ion beam axis is around 5×10^{-4} T.

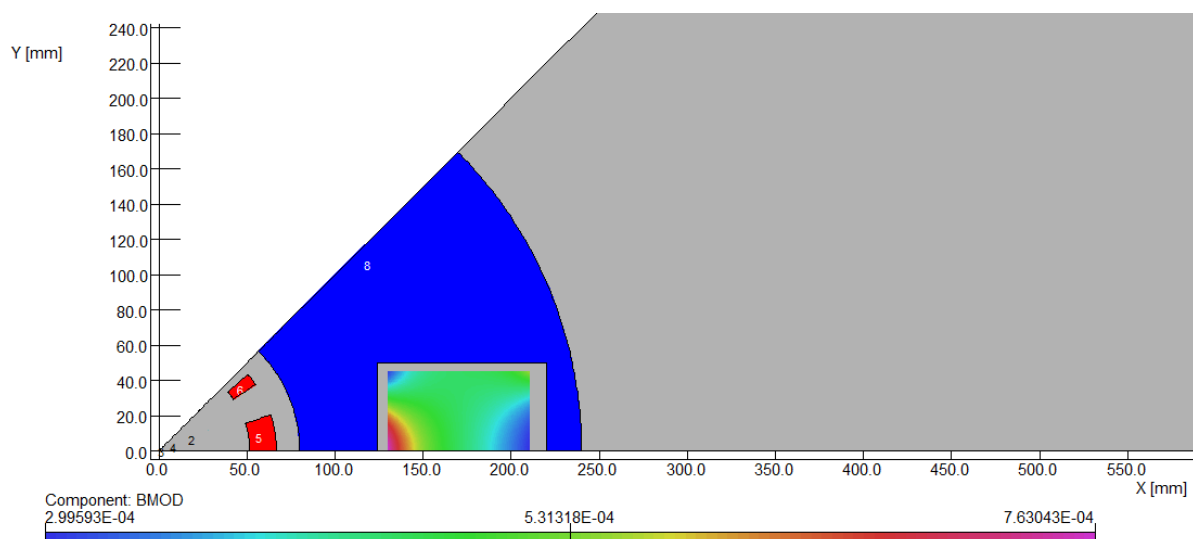


Fig.17. Field contour in the cutout of QFFUS_1 OPERA2d. The field magnitude is in the range of 10^{-4} T. (units are in millimeters and teslas).

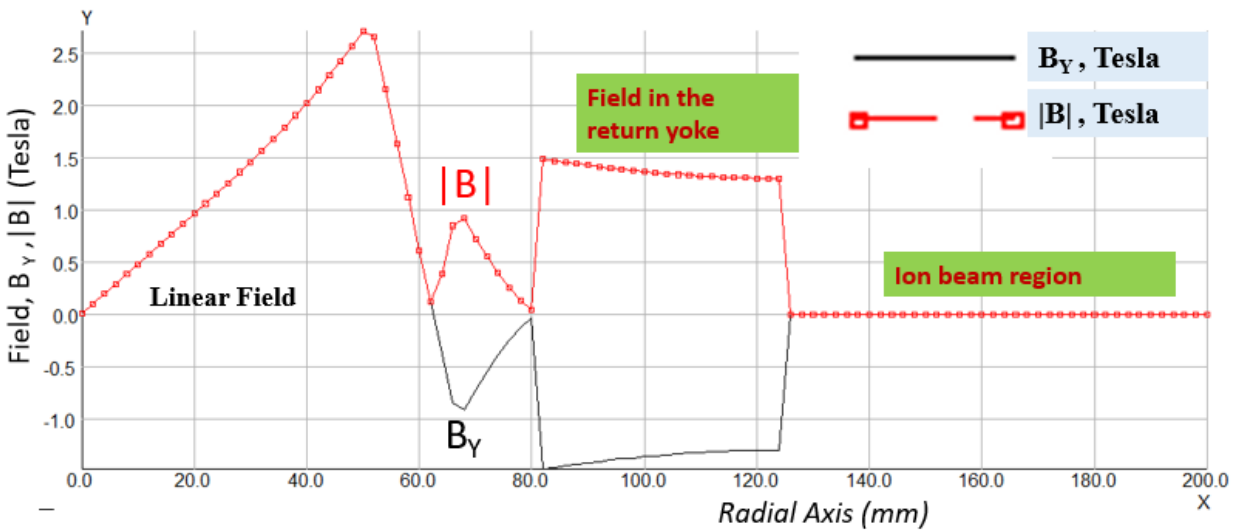


Fig.18. Profile of the calculated field components (B_Y and B_{MOD}) along the radial axis. The magnitude of the field at a radius of 0.032 m is 1.57 T, whereas the magnitude of the field at 180 mm is around 5×10^{-4} T.

Based on preliminary 2D modeling and analysis, a 3D solid model has been created. As per design parameters, the 3D model presumes inner and outer radius of the cryostat at 45 mm and 80 mm respectively. The advantage of the compact design makes it feasible to consider warm iron design. This will further simplify the assembly and the maintenance of the magnet around the ion beam line. Fig.19 shows a schematic layout for the quadrupole magnet with coils and cutout in the return yoke. Fig. 20 (left) shows schematic layout for two beam lines and (right) a 3D quadrupole magnet model with coils and ion beam line through the cutout in the return yoke.

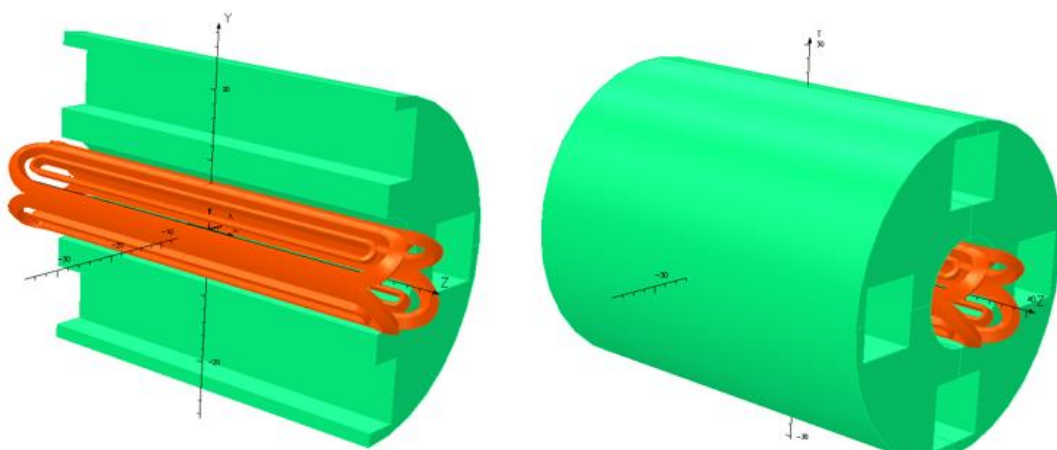


Fig.19. 3D solid model for superconducting QFFUS_1 quadrupole magnet with coils and warm iron return yoke.

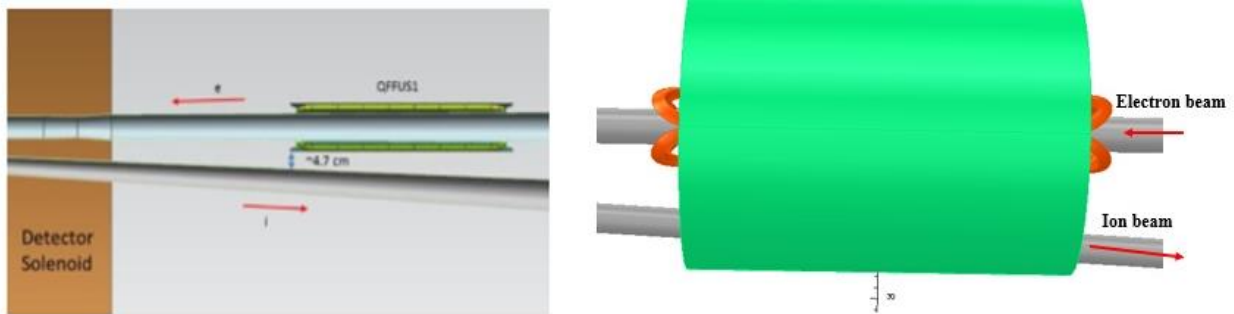


Fig.20. Schematic layout of the electron and ion beam lines with QFFUS_1 coils (left). Warm iron QFFUS_1 quadrupole magnet with ion beam pipe in the cutout (right).

4.0 Superconducting Shielding Options

Various superconducting shielding materials and shapes are being considered for this application. A return yoke and the passive superconducting shielding will be an integral part of the magnet cold-mass. Material such as low temperature superconductor (LTS) either in the form of sheet/tubes and high-temperature superconductor tube/tapes (either Bi2223, a first-generation superconductor, or rare-earth barium copper oxide (ReBCO), a second-generation superconductor) have been investigated as part of this program and are materials of interest. A practical advantage of HTS is that an experimental program in liquid nitrogen (LN₂) is simpler and more economical than in liquid helium.

5.0 Superconducting Shielding Tests

This section summarizes the experimental test results [17] of several options for the superconducting shielding during Phase I. These include 77 K tests of (a) two configurations of the High Temperature Superconducting (HTS) ReBCO tape and (b) two orientations of tube made with the HTS bulk material (Bi2223). A practical advantage of HTS for Phase I is that its basic configuration can be tested at a relatively low cost at 77 K.

PBL/BNL team collaborated with conductor manufacturers and was able to obtain conductor free of cost in return for sharing data and acknowledging their contributions. Fig. 21 shows a Bi2223 (HTS) tube 80 mm long, ~1.5 mm thick and 10 mm inner diameter, provided by CAN SUPERCONDUCTORS, s.r.o., a Czech company [18].



Fig.21. Bi2223 tube provided by CAN superconductor [18]. The tube and test holder will be inserted inside the bore of a coil providing background field.

In addition, limited shielding tests for both an HTS tube and an LTS tube were also performed at ~4 K, which was beyond what was promised by the Phase I proposal. This was possible thanks to a synergy with another ongoing magnet test at BNL which could accommodate such shielding tests. The ~4 K tests are very valuable to EIC, because the magnets will operate at ~4 K. As expected, 4 K provided shielding to much higher fields.

Fig. 22 (right) shows the NiTi rod provided by J. Parrell from Bruker [19] and Fig. 22 (right) the NbTi rod provided by H. Kanithi from Luvata [20]. Tubes for superconducting shielding tests were made from these rods by boring axially with a ½" (12.7 mm) drill as shown in Fig. 23. Both tubes were annealed at a temperature of 400 C for 4 hours in vacuum better than 10^{-5} torr at BNL.



Fig.22. NbTi rods for making LTS shielding tubes provided by Bruker [19] (right) and by Luvata [20] (left).

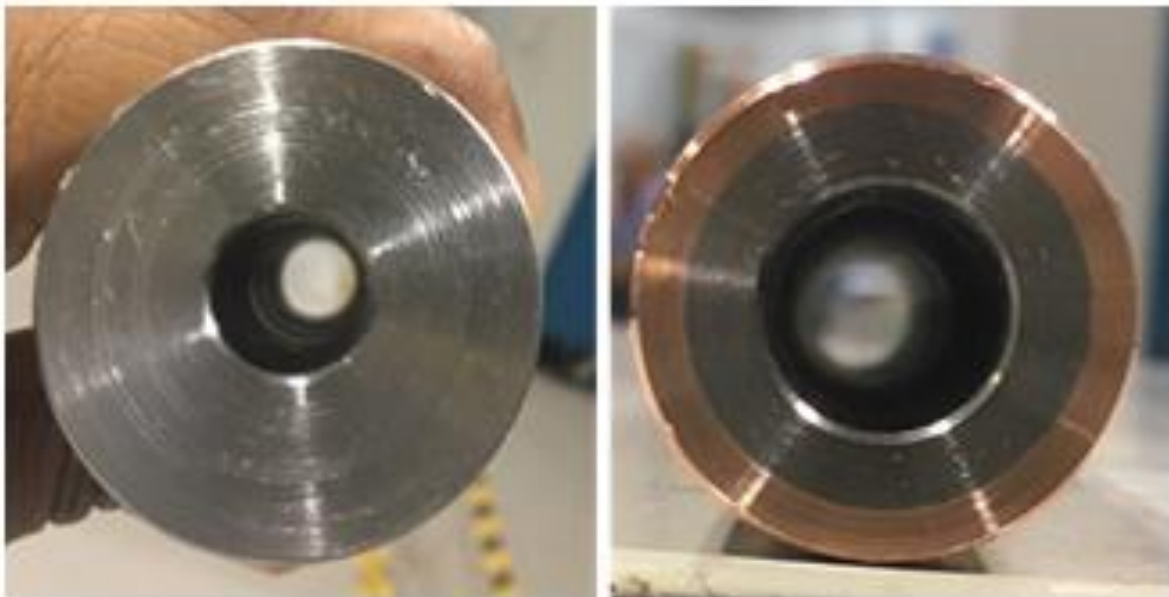


Fig.23. LTS tubes made from the NbTi rods provided by Bruker [19] (left) and by Luvata [20] (right). The inner diameter of both tubes is 12.7 mm.

The additional activities and tests demonstrate the interest and commitment of the PBL/BNL team towards developing the shielding technology for EIC magnets and other applications. It has allowed us to make a strong Phase II proposal to demonstrate this shielding development alongside a real superconducting quadrupole.

5.1 Shielding Tests with Spirally Wound HTS Tape at 77 K

The first configuration is a spirally wound HTS tape. We used 12 mm tape from SuperPower [21] wound on a stainless-steel tube, as shown in Fig. 24. Each spiral creates a small dipole with shielding current running parallel to the tube and in opposite direction on two sides, with the circuit completed with current running along the spiral using a partial width of the tape. The direction of current in two nearby spirals is opposite to each other and thus the axial field created by them essentially cancels out. Many small dipoles add together to provide complete shielding until the induced current in the tape reaches its critical value. Fig. 25 shows an insulation wrap, which also holds the tape together. Fig. 26 shows two views of a C-shaped dipole built specifically for this experiment with the leftover HTS coils from another project. Fig. 27 shows the demonstration of the shielding at the center of the tube against the applied field. A single wrap of ~12 mm wide HTS tape from SuperPower [21] is able shield a field of ~20 mT at 77 K.



Fig. 24: 12 mm wide HTS tape spirally wrapped around a tube.



Fig. 25: 12 mm wide HTS tape spirally wrapped around a tube and then further wrapped with insulation to hold it securely.

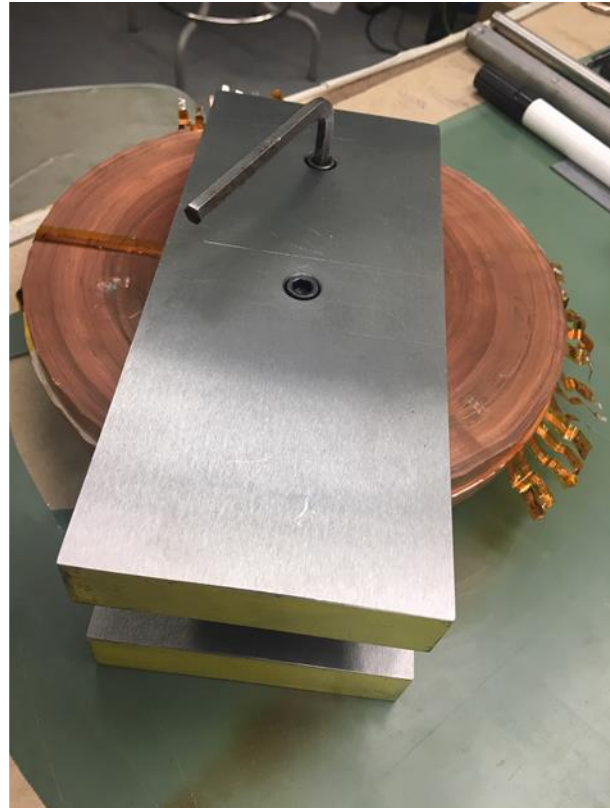


Fig. 26: Two views of a C-shaped dipole built with HTS coils for applying field primarily perpendicular to the tube for the test of shielding.

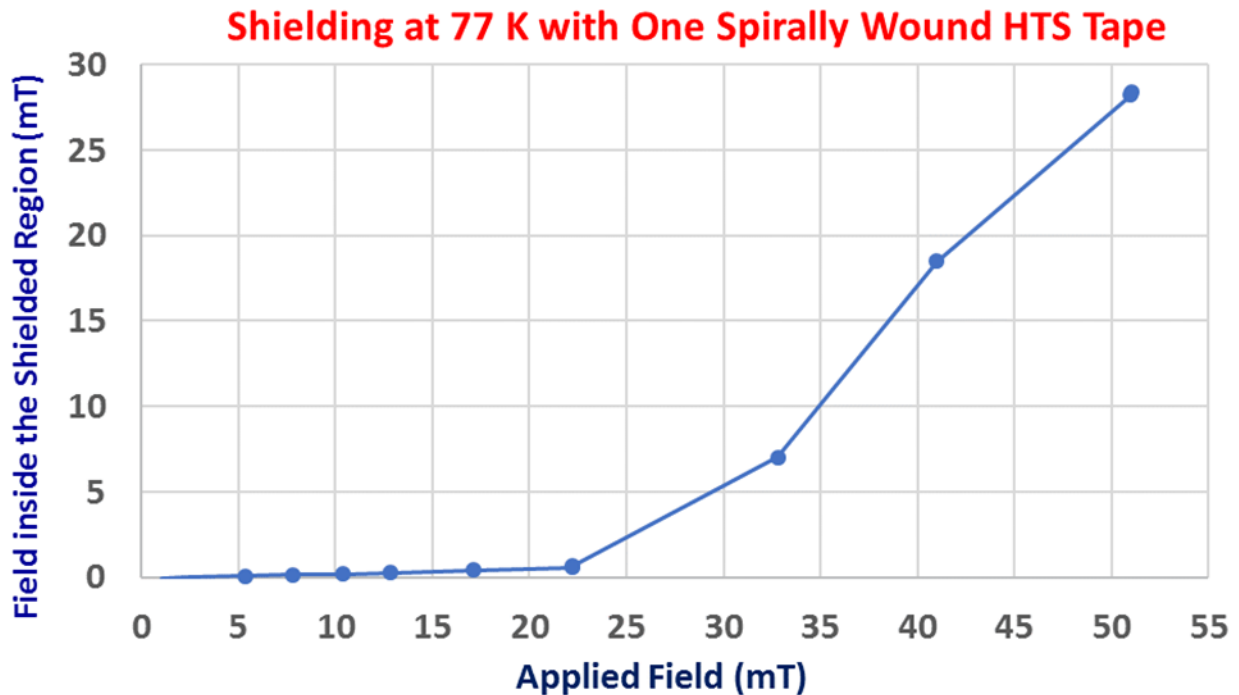


Fig. 27: Test results of field inside the tube as function of applied field, to simulate the beam tube in a dipole field with superconducting shielding.

5.2 Shielding Tests with Axially Wrapped HTS Tape at 77 K

We also examined the HTS tape wrapped around the tube axially. The widest tape available from the most HTS manufacturer is 12 mm wide, but American Superconductor Corporation [22] can provide it in ~40 mm width on special order. Fig. 28 shows the configuration when this 40 mm wide tape is placed on the tube with length parallel to the tube. It can create a long dipole with the shielding current running along the length of the tape if it rolls over the vertical axis to accommodate currents in opposite directions on the two sides. For shielding to work properly, the minimum width of the tape should be $\frac{1}{2}$ the circumference to shield a dipole field, and $\frac{1}{4}$ the circumference to shield a quadrupole field. Fig. 29 shows the results of our shielding experiment. The tape was folded in a tight radius (<10 mm) which might have degraded the shielding current it could support and therefore the shielding it could provide. The field inside the shield region, as shown in Fig. 29, was non-zero at the start. That is because the iron had been magnetized from the previous run, and generated an offset to the field applied from powering the coil. Superconducting shielding resist changes in field, and therefore can trap field, not merely exclude it. Fig. 29 shows several cases of different starting conditions.



Fig. 28: HTS tape placed on a tube to simulate the shielding test of a primarily dipole field along the beam axis.

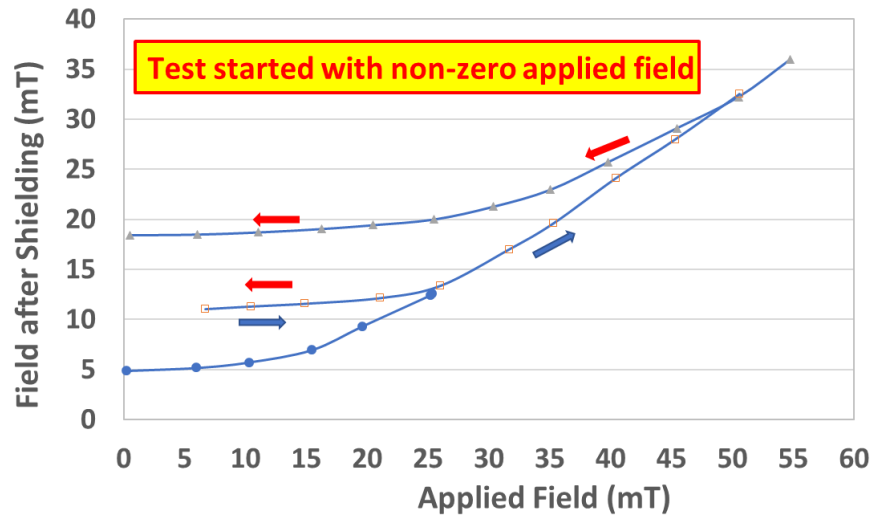


Fig. 29: Test results of shielding experiment when HTS tape placed on a tube to shield a primarily dipole field along the axis. This test demonstrates that a superconducting shield resists changes in field.

5.3 Shielding Tests with HTS Tube at 77 K

Measurements provided by an HTS tube were carried out at 77 K. Fig. 21 shows the Bi2223 (HTS) tube (80 mm long, ~1.5 mm thick and 10 mm inner diameter) from CAN Superconductors [18] in a holder. The shielding properties of an HTS tube depend on the direction of applied field. For a field that is primarily parallel, a copper coil was wound directly on the Bi2223 tube to create an axial field (see Fig. 30).



Fig. 30. Copper windings on the HTS tube to immerse it in a field that is primarily axial.

An existing 100 mm diameter double pancake HTS coil (see Fig. 31) was used to apply field in primarily the transverse direction to the tube when it is inserted inside and kept parallel to the double pancake.

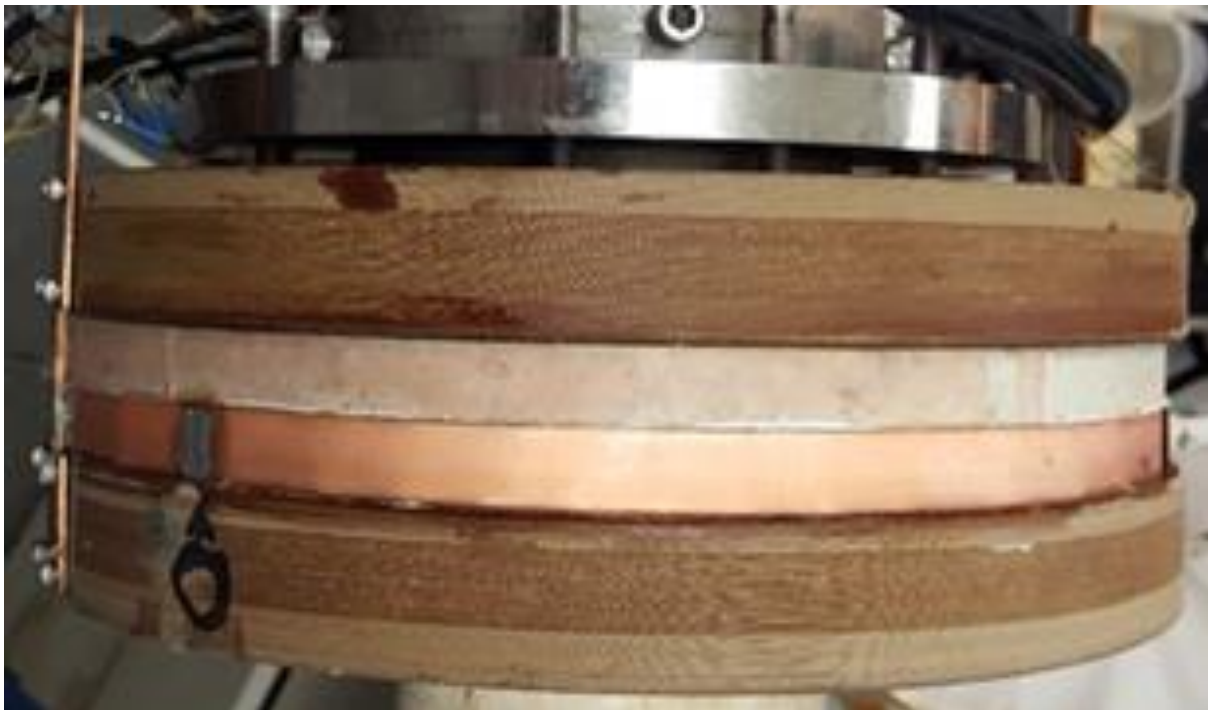


Fig. 31. HTS double pancake coil used to generate a field which is primarily in transverse direction over much of the volume of shielding tube.

Fig 32 shows the tube (with Hall probe installed at the center of the tube) in a flask into which liquid nitrogen can be poured.



Fig. 32: Bi2223 tube with copper windings on the HTS tube to apply a field that is primarily along the axis placed in the jar that is to be filled with liquid nitrogen with Hall probe placed at the center of the tube.

Fig. 33 shows the results of two hysteresis runs (1) with an ambient field primarily axial (blue) simulating the case field primarily parallel and (2) primarily radial (red) simulating the case field primarily perpendicular. The field inside the tube increases in step with the applied field once the field has reached the maximum that the tube can shield. When the applied field is decreased, the field inside the tube initially remains unchanged, because shielding currents oppose the change. Field inside the tube is trapped, leaving a residual field when the applied field has become zero.

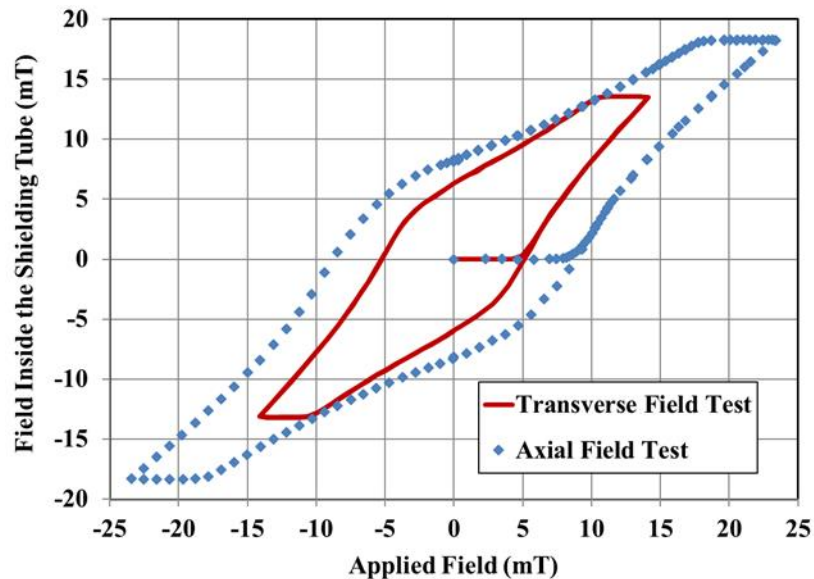


Fig. 33: Measured field at the center of the Bi2223 tube at 77 K with an ambient field primarily axial (blue) or primarily radial (red).

5.4 Shielding Tests with HTS and LTS Tubes at 4 K

The HTS (Bi2223) tube used in this experiment was provided by CAN SUPERCONDUCTORS, s.r.o., a Czech company [18]. It is 80 mm long and ~1.5 mm thick, with an inner diameter of 10 mm. The NbTi tube used in this shielding experiment was made from the ~20 mm diameter NbTi rod sent by Luvata [20]. It was clad with ~3 mm of copper and included a thin ($\ll 1$ mm) Nb barrier. Fig. 34 (left) and Fig. 34 (center) show views of the tubes of HTS (black) and LTS (copper clad). The two superconducting shielding tubes are off-axis, with the center of each tube located at $r = 20$ mm to 30 mm. Three Hall probes are installed, two at the center of each tube and one at the center of the HTS coil applying the background field. The shielding tube measurements were performed at several temperatures ranging from 4.2 K to 77 K.



Fig. 34: Pictures on the left and center show the two views of the HTS and LTS tubes and a center tube holding a Hall probe on the axis of the disc. The picture on the right shows the HTS and LTS shielding tubes inside an HTS coil with several Hall probes.

Fig. 35 shows the field at the center of the NbTi tube as a function of the applied field; the NbTi tube shields completely to about ~1.5 T. Beyond that, the current density needed to fully negate the applied field exceeds the superconducting properties of NbTi, and the tube quenches. However, the NbTi tube recovers and becomes superconducting again, resisting changes in field from 1.5 T; the tube traps field even if the applied field is turned off. The tube also resists further increases in field until the required current density exceeds the critical current density at a field that is higher by ~ 2.6 T – 1.5 T = 1.1 T. The second field increment is smaller than the first because the critical current density decreases with increasing field. The thicker the tube, the greater its ability to shield fields, because the required current density decreases. Of course, at fields exceeding the critical field of NbTi, the tube is not able to provide any shielding at all, whatever its thickness. The IR magnets of EIC need not shield a field as high as 1.5 T, so a thinner shield should suffice.

The 76 mm (3") long LTS tube was centered at the midplane of the coil. The applied field across the volume of the tube was far from uniform, varying across the radius and falling to nearly zero at the ends of the tube. We define the applied field as its maximum value.

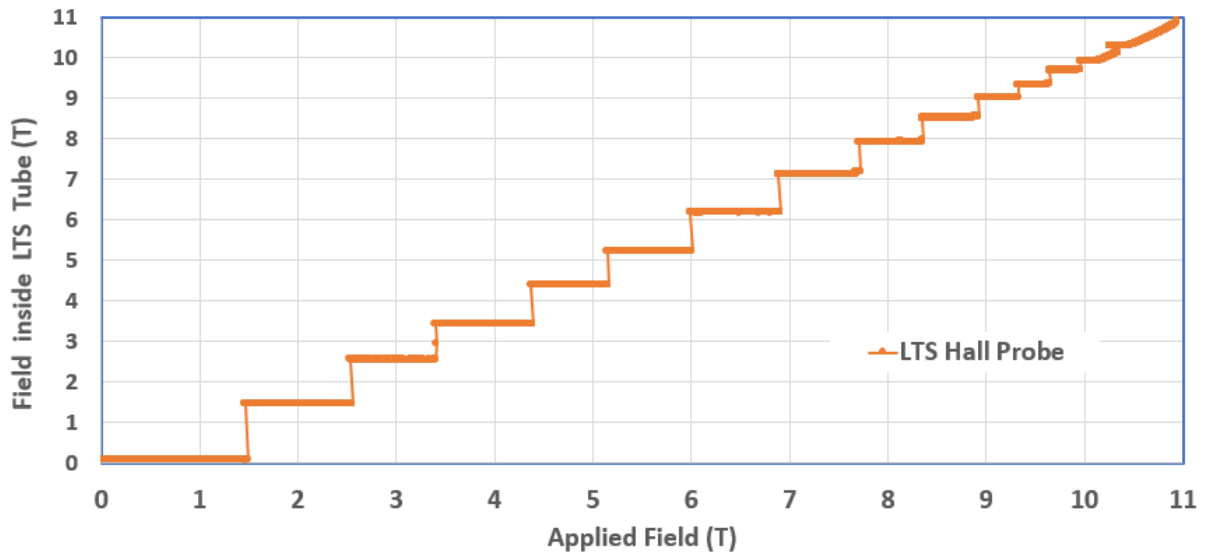


Fig. 35. Field inside the NbTi tube as a function of applied field. The shielding is complete up to ~ 1.5 T, thereafter trapping field. Steps are due to quenches in the NbTi tube, temporarily zeroing the trapped field trapped.

Fig. 36 shows the shielding properties of the Bi2223 HTS tube. Because the tube is much thinner (~ 1.5 mm), it shields much less (~ 0.12 T). However, because the current density of HTS at 4 K decreases very little with field, an HTS shield of sufficient thickness could, in principle, shield fields even higher than LTS.

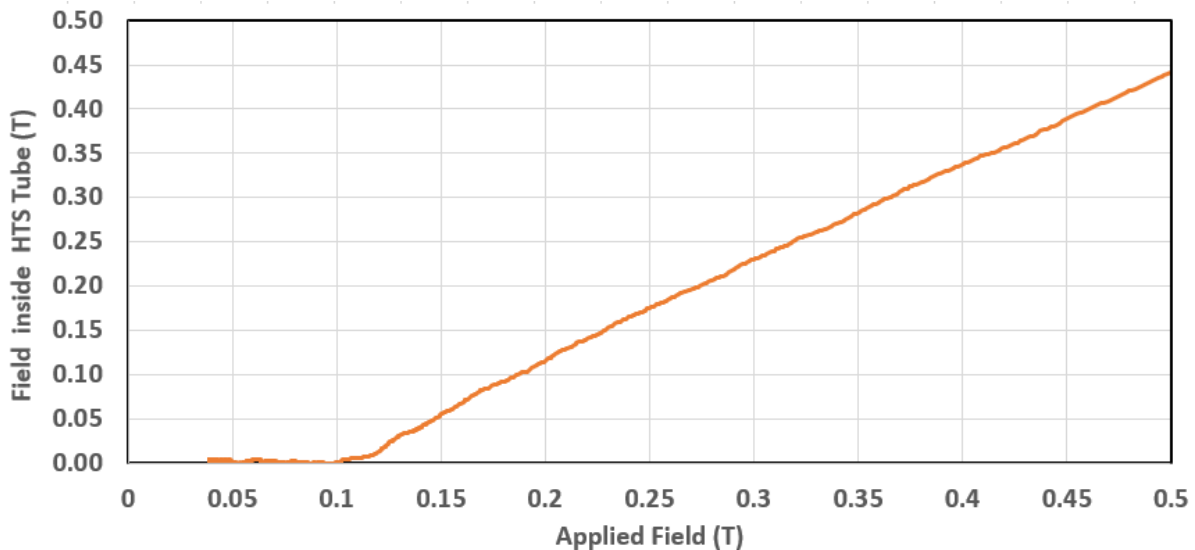


Fig. 36. Field inside the Bi2223 (HTS) tube as a function of the applied field. The shielding is complete up to ~ 0.12 T.

6.0 Prospects of Shielding in Various EIC Magnets

We have evaluated the prospects of shielding in various EIC magnets. The subject has been partly discussed in section 3 (magnetic design analysis). Computer models of the critical quadrupoles of both BNL and JLAB designs have been made and evaluated. In addition to the extensive evaluation of the Q1PF quadrupole in the BNL eRHIC design, we also reviewed the quadrupoles QFFUS1 and QFFB2. The models of these quadrupoles with shielding (as made at JLAB and reported in the recent ASC2018 paper [8]) are shown in Fig. 37. The picture on the left shows the OPERA3d model of QFFUS1, with passive shield over the electron beam (left-most green cylinder), quadrupole coils for ion beam, and active shield over quadrupole coils. The picture on the right shows the OPERA3d model of JLAB Quad QFFB2 (right) with the Quadrupole coil for ion beam, passive shield (green), active shield over the passive shield (green) and the iron yoke (blue) [8].

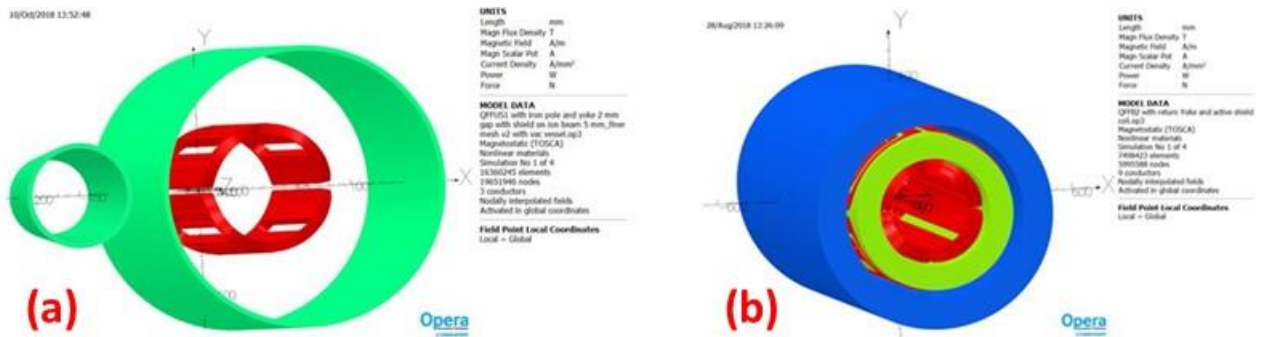


Fig. 37: (a) OPERA3d model of JLAB Quad QFFUS1 (left) [8] with passive shield over the electron beam (left-most green cylinder), quadrupole coils for ion beam, and active shield over quadrupole coils; (b) OPERA3d model of JLAB Quad QFFB2 (right) [8] with the Quadrupole coil for ion beam, passive shield (green), active shield over the passive shield (green) and the iron yoke (blue).

In addition to the quadrupole magnets, incorporation of superconducting shielding is particularly attractive in a spectrometer dipole (B0 in the BNL proposal of eRHIC) [23], in which an electron beam must traverse through the same dipole the proton or iron beam passes, but the electron beam must be shielding from the strong dipole field and be focused by the gradient of the quadrupole. Fig. 38 shows the basic design of spectrometer dipole B0 in the BNL proposal. The compensation dipole coil needs to be inside the magnet, with an appropriate field profile needed for both the electron beam and the proton or ion beam. Fig. 39 (left) shows the contour plot of field in the spectrometer dipole B0 for the eRHIC EIC proposal; Fig. 39 (right) shows the field profile outside the dipole coil, with the influence of the cancellation coil.

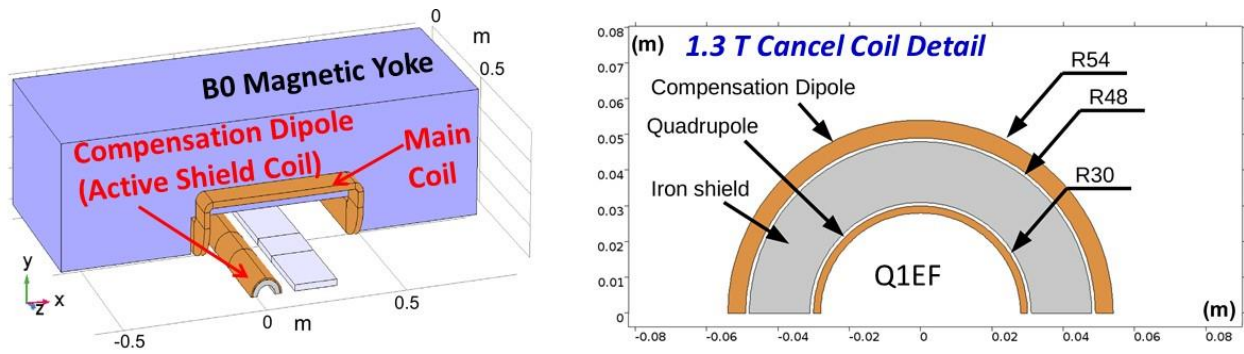


Fig. 38: Conceptual design of the spectrometer dipole B0 [23] for eRHIC EIC proposal. Shown on the left are the main coil, yoke and compensation dipole coil (also referred to as the active shield coil). In detail on the right are major elements of the quadrupole for the electron beam.

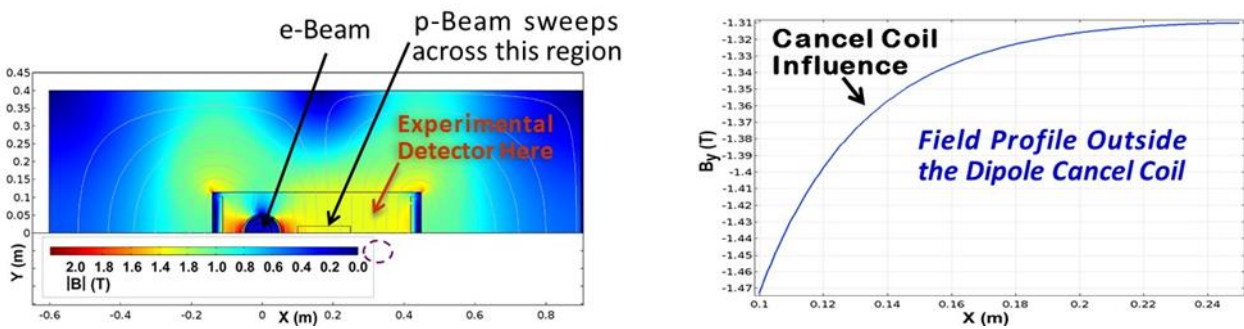


Fig. 39: Contour plot of field in the spectrometer dipole B0 [23] for the eRHIC EIC proposal, and field profile outside the dipole coil, with influence of the cancellation coil.

7.0 Planning of the Shielding Tests in Phase II

To perform the superconducting shielding experiments in Phase II at ~ 4 K in a long length magnet with shielding extending beyond the length of the magnet, we propose to use an existing quadrupole magnet at BNL which is shown in Fig. 40. The assembly has both quadrupole and sextupole windings; however, only the quadrupole windings will be energized. The picture on the left shows the two windings before the insulating wrap; the picture on the right shows the completed magnet with wrap, which also serves as the outer support structure to contain the Lorentz forces.



Fig. 40: Superconducting coil windings before (left) and after insulating and structural wrap (right) that will be used in providing the test field in Phase II.

The magnet does not have any yoke iron over the coil. A 3-D model of this magnet is shown in Fig. 41 (left); the field profile at the midplane as a function of distance is shown in Fig. 41 (right). The location of the superconducting shield can be adjusted during this experiment; in one of the tests it will be placed inside the magnet.

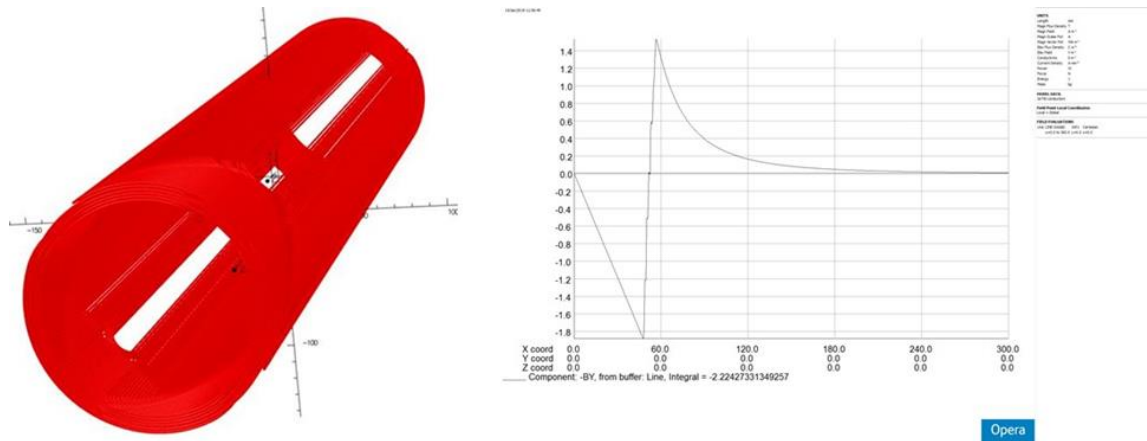


Fig. 41: 3-D model of the quadrupole magnet (see left) chosen for the shielding experiment in Phase II, and field profile at the midplane as a function of distance (right).

Fig. 42 and 43 shows the CAD models of the quadrupole, superconducting shield (with heaters shown over the superconducting shield to quench it during the experiment) and inside iron or low-retentivity material tube as mentioned in the proposal.

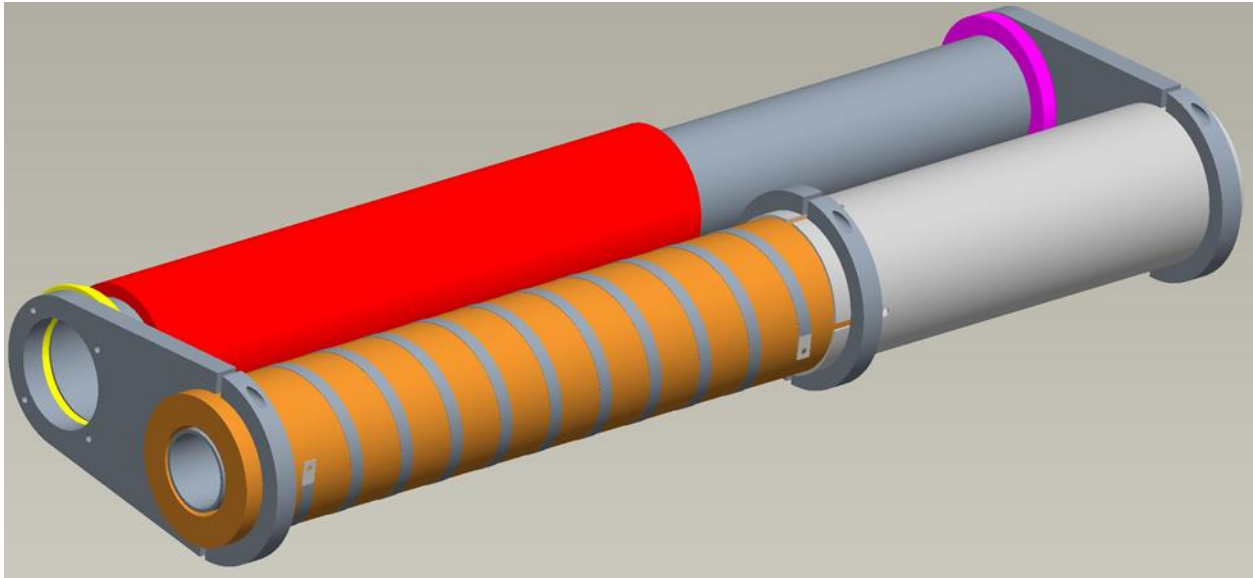


Fig. 42: CAD model of the quadrupole, superconducting shield with heaters over the superconducting shield (to quench it during the experiment) and inside iron tube along with the adapter plate.

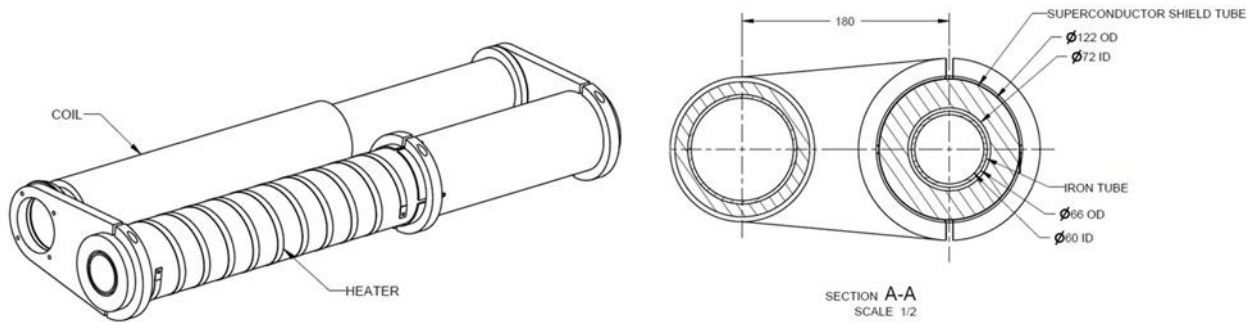


Fig. 43: Sketches and different views of the quadrupole, superconducting shield with heaters over the superconducting shield, inside iron tube with the adapter plate. The separation between the quadrupole and the shield can be adjusted by using different adapter plates.

8.0 Summary

We have evaluated the benefits of using passive superconducting shielding in several magnets for the proposed Electron Ion Collider (EIC). In addition to quadrupoles, it can also play an important role in the spectrometer dipole in the interaction region. The machine designs of both options (JLEIC being pursued at the Jefferson Lab, and eRHIC at BNL) are still evolving, and therefore it was appropriate to develop and demonstrate the technology in the range of interest rather than a specific magnet. Phase II, also, is planned with that consideration.

Significant progress has been made by the PBL and BNL team, including key demonstrations, some beyond the original scope of Phase I. In addition to analyzing the computer models of specific magnets, we also summarized the extensive experimental test results of several options for the superconducting shielding. These include 77 K tests of (a) two configurations of the High Temperature Superconducting (HTS) ReBCO tape and (b) two orientations of tube made with the HTS bulk material (Bi2223). A practical advantage of HTS for Phase I is that its basic configuration can be tested at a relatively low cost at 77 K. Existing HTS coils were used by themselves and in making a C-shaped dipole magnet (see Fig. 9) to perform these tests.

PBL/BNL team collaborated with conductor manufacturers, who generously donated a shielding tube made of bulk material (Bi2223) from CAN SUPERCONDUCTORS, s.r.o., a Czech company and NbTi rods from which to make LTS tubes at BNL from Oxford Superconductors and Luvata.

These additional activities and tests demonstrate the interest and commitment of the PBL/BNL team towards developing the shielding technology for EIC magnets and other applications. It has also allowed us to make a strong Phase II proposal to demonstrate this shielding development alongside a real superconducting quadrupole.

9.0 References

1. Nuclear Science Advisory Committee (NSAC) is an advisory committee that provides official advice to the Department of Energy (DOE) and the National Science Foundation (NSF) on the national program for basic nuclear science research. <https://science.energy.gov/np/nsac/>
2. 2015 NSAC Long Range Plan “*Reaching for the Horizon*”, October 20, 2015. https://science.energy.gov/~media/np/nsac/pdf/2015LRP/2015_LRPNS_091815.pdf
3. RHIC | Electron-Ion Collider - Brookhaven National Laboratory <https://www.bnl.gov/rhic/eic.asp>
4. JLEIC Design - Electron Ion Collider Wiki https://eic.jlab.org/wiki/index.php/Main_Page
5. EIC Collaboration Meeting 2017 at Brookhaven National Laboratory, Oct. 10-12, 2017. <https://indico.bnl.gov/conferenceDisplay.py?confId=3492>
6. 2018 EIC Accelerator Collaboration Meeting, <https://www.jlab.org/indico/event/281/>, Thomas Jefferson National Accelerator Facility (TJNAF), Newport News, Virginia, 29 October 2018 to 1 November 2018.
7. B. Parker “*Fast Track Actively Shielded Nb₃Sn IR Quadrupole R&D*”, Oct 11, 2017 <https://indico.bnl.gov/getFile.py/access?contribId=28&sessionId=5&resId=1&materialId=slides&confId=3492>
8. R. Rajput-Ghoshal, R. Fair, P. K. Ghoshal, C. Hutton, E. Sun, M. Wiseman, “Preliminary Design of the Interaction Region Magnets for Future Electron-Ion Collider at Jefferson Lab,” 2018 Applied Superconductivity Conference, Seattle, October 28 - November 2, 2018.
9. Opera Electromagnetic FEA Simulation Software, <https://operafea.com/>.
10. ROXIE – CERN, <https://cern.ch/roxie>.
11. A. Yamamoto, et al. “*The superconducting inflector for the BNL g-2 experiment*,” Nuclear Instruments and Methods in Physics Research A 491 (2002) 23–40.
12. K.G. Capobianco-Hogan, et al. “*Magnetic field cloak for charged particle beams*,” Nuclear Inst. and Methods in Physics Research, A 877 (2018) 149–156.
13. A. Deshpande, N. Feege, R. Gupta, “*A Magnetic Field Cloaking Device for Applications with Strong Magnetic Fields*,” SBU/BNL Seed Grant Proposal (unpublished), April 2015.
14. A. Koski and S.L. Wipf, “*Magnetic shielding of an accelerator beam using passive ferromagnetic material*,” IEEE Trans. Magnetics, vol. 32, pp. 2663–2666, 1996.
15. D. Barna, “High field septum magnet using a superconducting shield for the Future Circular Collider,” Phys. Rev. Accel. Beams, vol. 20, no. 4, p. 041002, 2017. [Online]. Available: <http://link.aps.org/doi/10.1103/PhysRevAccelBeams.20.041002>.
16. P. Ferracin, et al., “Development of a large aperture Nb₃Sn racetrack quadrupole magnet”, IEEE Trans. Appl. Superconductivity, Vol. 15, No. 2, pp. 1132-1135, June 2005.
17. R. Gupta, S. Joshi, B. Parker, W. Sampson, S. Chouhan, S. Kahn, J. Kolonko, D. Larson, R. Scanlan, R. Weggel and E. Willen, “Field Compensation in Electron-Ion Collider Magnets with a Passive Superconducting Shield,” 2018 Applied Superconductivity Conference, Seattle, October 28 - November 2, 2018.
18. Jan Plecháček, CAN Superconductors, s.r.o., <https://www.can-superconductors.com>, Czech Republic.
19. J. Parrell, <https://www.bruker.com/>.
20. H. Kanithi, <http://www.luvata.com/waterbury>, USA.
21. SuperPower, Inc. <http://www.superpower-inc.com/>.
22. American Superconductor (AMSC), <https://www.amsc.com/>.
23. Holger Witte and Brett Parker, BNL, Private Communication, “eRHIC: B0 Spectrometer”, also presented at EIC Accelerator Collaboration Meeting, <https://www.jlab.org/indico/event/281/>.